

AD-A173 813

STIRLING ENGINE EXTERNAL HEAT SYSTEM DESIGN WITH HEAT
PIPE HEATER(U) STIRLING THERMAL MOTORS INC ANN ARBOR MI
T M GODETT ET AL JUL 86 AFMNL-TR-86-2018

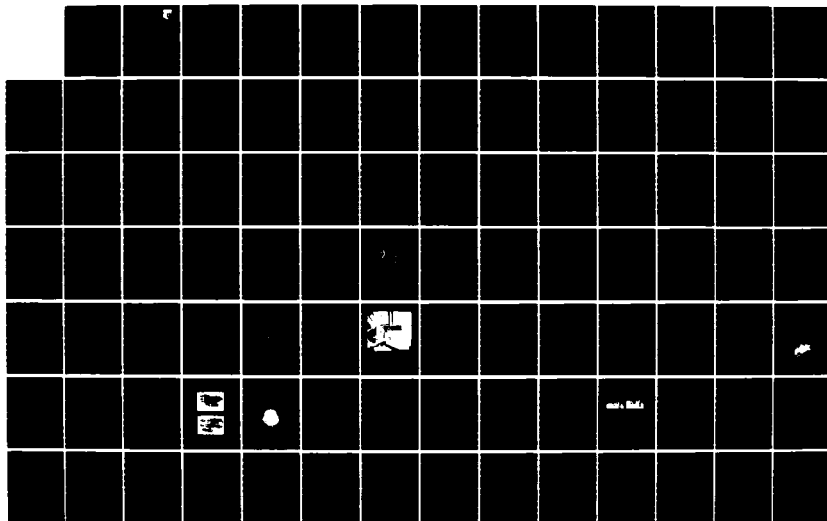
1/2

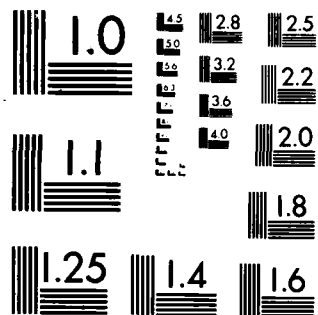
UNCLASSIFIED

MIPR-FV-1455-B4-N0618

F/G 21/7

NL



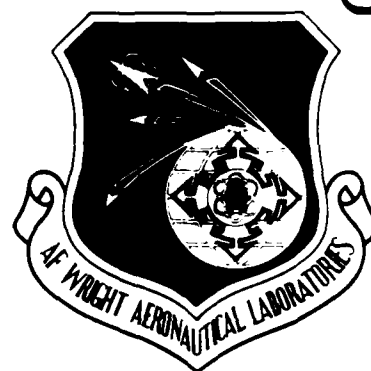


MICROCOPY RESOLUTION TEST CHART
NATIONAL BUREAU OF STANDARDS-1963-A

2

AFWAL-TR-86-2018

**STIRLING ENGINE EXTERNAL HEAT SYSTEM DESIGN
WITH HEAT PIPE HEATER**



Ted M. Godett
Benjamin Ziph
Stirling Thermal Motors, Inc.
2841 Boardwalk
Ann Arbor, MI 48104

July 1986

Final Report for Period April 1984 - December 1985

Approved for Public Release; Distribution is Unlimited

AD-A173 813

DTIC FILE COPY

AERO PROPULSION LABORATORY
AIR FORCE WRIGHT AERONAUTICAL LABORATORIES
AIR FORCE SYSTEMS COMMAND
WRIGHT-PATTERSON AIR FORCE BASE, OHIO 45433-6563

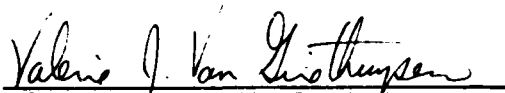


86 11 080

NOTICE

When Government drawings, specifications, or other data are used for any purpose other than in connection with a definitely related Government procurement operation, the United States Government thereby incurs no responsibility nor any obligation whatsoever; and the fact that the government may have formulated, furnished, or in any way supplied the said drawings, specifications, or other data, is not to be regarded by implication or otherwise as in any manner licensing the holder or any other person or corporation, or conveying any rights or permission to manufacture, use, or sell any patented invention that may in any way be related thereto.

This technical report has been reviewed and is approved for publication.



VALERIE J. VAN GRIETHUYSEN
Project Engineer
Power Technology Branch
Aerospace Power Division



JERRELL M. TURNER
Chief
Power Conversion Project Office
Aerospace Power Division

FOR THE COMMANDER:



JAMES D. REAMS
Chief, Aerospace Power Division
Aero Propulsion Laboratory

If your address has changed, if you wish to be removed from our mailing list, or if the addressee is no longer employed by your organization please notify AFWAL/POOA, W-P AFB, OH 45433 to help maintain a current mailing list.

Copies of this report should not be returned unless return is required by security considerations, contractual obligations, or notice on a specific document.

Unclassified

SECURITY CLASSIFICATION OF THIS PAGE

AD-A173 813

REPORT DOCUMENTATION PAGE

1a. REPORT SECURITY CLASSIFICATION Unclassified		1b. RESTRICTIVE MARKINGS										
2a. SECURITY CLASSIFICATION AUTHORITY		3. DISTRIBUTION/AVAILABILITY OF REPORT Approved for public release; distribution is unlimited.										
2b. DECLASSIFICATION/DOWNGRADING SCHEDULE												
4. PERFORMING ORGANIZATION REPORT NUMBER(S)		5. MONITORING ORGANIZATION REPORT NUMBER(S) AFWAL-TR- 86-2018 NASA Contractor Report No. CR175065										
6a. NAME OF PERFORMING ORGANIZATION Stirling Thermal Motors, Inc.	6b. OFFICE SYMBOL (If applicable)	7a. NAME OF MONITORING ORGANIZATION Aero Propulsion Laboratory (AFWAL/POOS) Air Force Wright Aeronautical Laboratories										
6c. ADDRESS (City, State and ZIP Code) Stirling Thermal Motors, Inc. 2841 Boardwalk Ann Arbor, MI 48104		7b. ADDRESS (City, State and ZIP Code) Wright - Patterson AFB OH 45433 - 6563										
8a. NAME OF FUNDING/SPONSORING ORGANIZATION	8b. OFFICE SYMBOL (If applicable)	9. PROCUREMENT INSTRUMENT IDENTIFICATION NUMBER MIPR #FY 1455 - B4 - NO618										
8c. ADDRESS (City, State and ZIP Code)		10. SOURCE OF FUNDING NOS. <table border="1"><tr><td>PROGRAM ELEMENT NO. 62203F</td><td>PROJECT NO. 3145</td><td>TASK NO. 24</td><td>WORK UNIT NO. 27</td></tr></table>		PROGRAM ELEMENT NO. 62203F	PROJECT NO. 3145	TASK NO. 24	WORK UNIT NO. 27					
PROGRAM ELEMENT NO. 62203F	PROJECT NO. 3145	TASK NO. 24	WORK UNIT NO. 27									
11. TITLE (Include Security Classification) Stirling Engine External Heat System Design with Heat Pipe Heater												
12. PERSONAL AUTHOR(S) Ted M. Godett and Benjamin Ziph												
13a. TYPE OF REPORT Final Report	13b. TIME COVERED FROM April '84 TO Dec. '85	14. DATE OF REPORT (Yr., Mo., Day) July 1986	15. PAGE COUNT 112									
16. SUPPLEMENTARY NOTATION												
17. COSATI CODES <table border="1"><tr><th>FIELD</th><th>GROUP</th><th>SUB. GR.</th></tr><tr><td>10</td><td>01</td><td></td></tr><tr><td>16</td><td>02</td><td></td></tr></table>		FIELD	GROUP	SUB. GR.	10	01		16	02		18. SUBJECT TERMS (Continue on reverse if necessary and identify by block number) External heating system, Stirling engine, Stirling cycle, heat pipes, heat exchangers, heat transfer, indirect heating, evaporator, evaporator fins, preheater, recuperator, sodium heat pipes	
FIELD	GROUP	SUB. GR.										
10	01											
16	02											
19. ABSTRACT (Continue on reverse if necessary and identify by block number) * This final report presents the conceptual design of a liquid fueled external heating system (EHS) and the preliminary design of a heat pipe heater for the STM4-120 Stirling cycle engine, to meet the Air Force mobile electric power (MEP) requirement for units in the range of 20 to 60 kW. The EHS conceptual design consists of a liquid fuel combustor, with a flat plate, counter flow recuperator and a corrugated, flat-surface heat exchanger that is the evaporator of a sodium heat pipe. The EHS design had the following constraints: (1) Packaging requirements limited the overall system dimensions to about 330mm x 250mm x 100 mm. (2) Heat flux to the sodium heat pipe evaporator was limited to an average of 100 kW/m and a maximum of 550 kW/m based upon previous experience. (3) The heat pipe operating temperature was specified to be 800°C based upon heat input requirements of the STM4-120. An analysis code was developed to optimize the EHS performance parameters and an analytical (over)												
20. DISTRIBUTION/AVAILABILITY OF ABSTRACT UNCLASSIFIED/UNLIMITED <input checked="" type="checkbox"/> SAME AS RPT. <input type="checkbox"/> DTIC USERS <input type="checkbox"/>		21. ABSTRACT SECURITY CLASSIFICATION Unclassified										
22a. NAME OF RESPONSIBLE INDIVIDUAL Valerie J. van Griethuysen		22b. TELEPHONE NUMBER (Include Area Code) 451 31255-2089	22c. OFFICE SYMBOL AFWAL/POOS-3									

DD FORM 1473, 83 APR

EDITION OF 1 JAN 73 IS OBSOLETE.

Unclassified

SECURITY CLASSIFICATION OF THIS PAGE

TABLE OF CONTENTS

SECTION	PAGE
I. INTRODUCTION	1
II. EXTERNAL HEATING SYSTEM CONCEPTUAL DESIGN	4
1. External Heating System Conceptual Design	4
2. System Analysis and Optimization	8
a. Description of the System Analysis Code	8
b. Results of the System Analysis and Optimization	10
III. HEAT PIPE PRELIMINARY DESIGN	22
1. Heat Pipe Theory	22
a. Hydrodynamics	22
1. Capillary Head	23
2. Liquid Pressure Drop	24
3. Vapor Pressure Drop	26
4. Body Force Head	27
5. Capillary Pumping Limit	28
6. Entrainment Limit	28
7. Sonic Limitation	30
b. Heat Transfer	30
1. Boiling Limitation	31
2. Heat Pipe Temperature Characteristics	31
(a) Temperature Drop Across the Evaporator Wall	32
(b) Temperature Drop Across the Saturated Wick	32
(c) Temperature Drop Due to Vapor Flow Resistance	33
(d) Temperature Drop Across the Condenser Tubes	33
2. Heat Exchanger/Evaporator Configuration	33
3. Analysis of the Heat Exchanger/Evaporator	39
IV. EXTERNAL HEATING SYSTEM CONSTRUCTION	46
1. Construction of the EHS Heat Exchanger/Evaporator	46
2. Construction of the EHS Recuperator	49
3. EHS Preliminary Design Drawings	49
4. Heat Exchanger/Evaporator Scale Model Tests	49
V. CONCLUSIONS	51

TABLE OF CONTENTS

SECTION	PAGE
REFERENCES	54
Appendix A - "Breakthrough in Energy Conversion	55
Appendix B - Preheater and Evaporator Heat Transfer Analysis	83
Appendix C - EHS Analysis Code Sample Run	89
Appendix D - Development of EHS Evaporator Pressure Drop Equations	95
Appendix E - Preliminary Design Drawings	101

LIST OF FIGURES

FIGURE		PAGE
1	External Heating System Schematic Illustration	6
2	Packaging Requirements of the EHS	7
3	Effect of Area Ratio on EHS Efficiency	11
4	Effect of Area Ratio on EHS Cold Start Fuel Consumption	12
5	Effect of Total Heat Transfer Area on EHS Efficiency	14
6	Effect of Total Heat Transfer Area on EHS Flow Friction Power	15
7	Effect of Total Heat Transfer Area on EHS Cold Start Fuel Consumption	16
8	Effect of Gap Width on EHS Efficiency	17
9	Effect of Gap Width on EHS Flow Friction Power	18
10a	Steady State Temperature Profile in STM4-120 EHS	21
10b	Flow Path Through STM4-120 EHS	21
11	Schematic Representation of STM4-120 Heat Pipe	34
12	Medium Weight Conoseal Joint with T-Bolt Quick Coupler	36
13	Schematic Representation of Heat Exchanger/Evaporator	38
14a	Fluid Streamlines in a Typical Evaporator Fin with Varying Heat Flux	40
14b	Fluid Streamlines in a Typical Evaporator Fin with Constant Heat Flux	40
15	Liquid and Vapor Pressure for a Typical Fin in the STM4-120 EHS Evaporator	42
16	Forming the EHS Evaporator Structure	46
17	Resulting Fin Shape After Squaring and Crimping	47
18	Shape and Fit of EHS Evaporator Plenum Walls to Fin Roots	48
19	Scale Model of Heat Exchanger/Evaporator	50
D-1	EHS Heat Exchanger/Evaporator Geometry	98

LIST OF TABLES

Table 1	Comparison of a Single Path and multi Parallel Paths Heat Exchangers of Equal Total Heat Transfer Area	9
Table 2	STM4-120 EHS Performance Data	20
Table 3	Heat Exchanger/Evaporator Construction and Performance Data	44

List of Symbols and Abbreviations

A, A_w	Wick cross-sectional area
A_v	Flow area of vapor core
K	Permeability
L	Length
N	Mesh size for screen-wires per inch
P	Pressure
Q	Heat transfer rate; total axial heat transport
Q_{CL}	Axial heat transport at capillary pumping limit
Q_e	Axial heat transport at entrainment
Q_s	Axial heat transport at sonic limit
Q_{BL}	Axial heat transport at boiling point
R, R_1, R_2	Meniscus radii of curvature
Re_l	Liquid Reynolds number
Re_v	Vapor Reynolds number
R_u	Universal gas constant
S	Crimping factor for screens
T	Temperature
T_l	Liquid temperature
T_v	Vapor temperature
V	Volume; velocity of vapor
V_s	Sonic velocity of vapor
we	Weber number
d	Wire or fiber diameter
f_l	Liquid frictional drag coefficient

f_v	Vapor frictional drag coefficient
g	Magnitude of gravitational acceleration field
h	Coefficient of heat transfer
k	Thermal conductivity
k_{eff}	Effective thermal conductivity of saturated wick
k_l	Thermal conductivity of saturated liquid heat pipe working fluid
k_w	Thermal conductivity of solid wick material
m_l	Liquid mass flow rate
m_v	Vapor mass flow rate
q	Heat flux
r_1	Condenser tube inside radius
r_2	Condenser tube outside radius
r_c	Effective capillary radius
r_h	Hydraulic radius
r_v	Radius of vapor core
w	Wire spacing of screen mesh
x, y	Length, position
ΔP_b	Body force head
ΔP_c	Net capillary head
ΔP_g	Hydrostatic head
$\Delta P_g, \Delta P_{gl}$	Components of hydrostatic head parallel and perpendicular to heat pipe axis
ΔP_i	Interfacial pressure difference
ΔP_l	Liquid pressure drop
ΔP_v	Vapor pressure drop
ΔT	Temperature difference

β	Profile coefficient for momentum flow
ϵ	Wick porosity
θ	Angle of heat pipe axis with respect to acceleration field vector
λ	Latent heat of vaporization
μ_l	Liquid viscosity
μ_v	Vapor viscosity
ρ_l	Liquid density
ρ_v	Vapor density
σ	Surface tension

SECTION I

INTRODUCTION

In a 1984 study the Energy Conversion Branch of the U.S. Air Force Wright Aeronautical Laboratories Aero Propulsion Laboratory investigated the use of advanced power generating devices for future mobile electric power (MEP) applications. One conclusion of that study was that kinematic Stirling engines have a high potential for meeting the requirements for mid-sized (30-100 kW) flightline and operational system electronics support applications.

There are several kinematic Stirling engines currently under development by various organizations. An example is the automotive Stirling engine now being developed under the Department of Energy (DOE) Automotive Heat Engine Program with program management by NASA Lewis Research Center. One current effort also sponsored by this DOE program is Contract DEN3-351 with Stirling Thermal Motors, Inc. (STM) of Ann Arbor, Michigan, to experimentally evaluate advanced Stirling concepts [1]. STM, using primarily private funding, has designed, and is fabricating, a Base Technology Stirling Engine, designated the STM4-120 (4 cylinders, 120 cc swept volume per cylinder), incorporating these advanced concepts. The STM4-120 design is suitable for a variety of applications and since its heat input is from a liquid metal heat pipe it can be connected easily to almost any heat source.

The STM4-120 design features several advanced concepts which should reduce the Stirling engine size, weight, complexity and expected manufacturing costs. Indirect heating technology, incorporating heat pipes, is an integral part of the STM4-120, making it possible to divide the engine into

an energy conversion unit (ECU) and a distinctly separate external heating system (EHS), thus permitting simplification of the heat exchanger design. The heater of the ECU, actually the uniform temperature condenser of the EHS heat pipe, is designed to take advantage of the high film coefficient of the condensing metal vapor. This permits design optimization based on Stirling cycle thermodynamic requirements, and not on flue gas heat transfer, resulting in improved engine performance.

Other advanced features, such as the variable angle swashplate power control and compliantly mounted reciprocating seals, are presented in the literature [2].

An analysis by Argonne National Laboratory looked specifically at the STM4-120's Air Force MEP applicability and concluded that such use is attractive [3].

These two studies and the STM4-120 design, led the Air Force Wright Aeronautical Laboratories to sponsor an additional task to the current DOE sponsored activity at STM. The new Air Force sponsored task was to design the external heating system for the STM4-120, which would meet the appropriate military specifications, MIL-STD-633 and MIL-G-52884 for a 30 kW mobile electric power generator set.

The STM4-120 was designed to produce about 40 kW (53 HP) at 3000 RPM. The Air Force has an MEP requirement for a range of 20 to 60 kW. Although the STM4-120 will produce approximately 25 kW (33 HP) at 1800 RPM, the heating system will be designed to the full rated power of 40 kW. The eventual reoptimization of the STM4-120 to produce the military required power at 1800 RPM is a straightforward procedure and will have relatively little impact on the external heating system design. A complete description

of the STM4-120 is included in Appendix A.

The Air Force Wright Aeronautical Laboratories requested NASA Lewis Research Center to undertake program management responsibility through Military Interdepartmental Purchase Request Number FY 1455-84-NO618, to expand the effort at STM to include the conceptual design of an external heating system and the preliminary design of a heat pipe heater for a Stirling powered electrical generator set.

SECTION II

EXTERNAL HEATING SYSTEM CONCEPTUAL DESIGN

1. EXTERNAL HEATING SYSTEM CONFIGURATION

The conceptual design of the external heating system (EHS) was based on the heat input requirements of the STM4-120 Base Technology Stirling Engine. The EHS was designed to operate on liquid fuel, using a flat plate, counter flow recuperator and a corrugated, flat-surface heat exchanger. In both components the flow of air and flue gas is strictly laminar (Poiseuille flow between flat plates) and hence the Nusselt number is independent of the Reynolds number. The Nusselt number based on gap hydraulic diameter, is taken to be always 7.6 [4].

The combustion chamber design was chosen from an existing Philips Stirling engine, the ADVENCO 4-88. The burner, atomizing air nozzle and mixing chamber were readily adaptable to the EHS design concept regarding fuel, size and performance.

In operation, preheated air is mixed with atomized fuel in the combustion chamber and burns continuously. The atomized fuel is introduced into the combustion chamber through a nozzle. The geometry of the combustion chamber was designed for proper mixing and distribution of flue gas flow into the heat exchanger. Primary air is fed into the combustion chamber through a swirl chamber and secondary air is fed downstream through radial holes. Film cooling further downstream prevents overheating of the combustion chamber walls.

Hot flue gas flows from the combustion chamber through the multiple parallel gaps of the heat exchanger, transferring its heat through the wall

into the finned enclosure. The enclosure is the evaporator section of a heat pipe where liquid sodium in the wick lining the inside wall evaporates. The sodium vapor flows to the engine via connecting tubes.

Since the evaporator enclosure was designed to operate at sub-atmospheric pressure, coarse wire mesh was incorporated to provide structural support to the fin walls, while providing a vapor path for the sodium working fluid.

The residual heat of the flue gas leaving the heat exchanger is used to preheat the incoming combustion air in the recuperator.

A schematic diagram of the EHS is shown in Figure 1. Due to the use of heat pipes for heat transport the EHS can be located a variety of locations relative to the STM4-120 ECU.

An analysis and simulation code for the EHS was developed to determine the influence of various geometric parameters on the system performance. The range of parameter variation was limited by the following considerations:

- Packaging requirements limited the overall system dimensions to about 330 mm x 250 mm x 100 mm as shown in Figure 2.
- Heat exchanger (evaporator) fins and preheater plates were designed with the same depth for ease of fabrication and packaging convenience.
- In laminar flow heat exchangers the Nusselt number can be assumed to be independent of the Reynolds number, therefore it was advantageous to divide the flow path into as many parallel paths as possible, to derive the maximum reduction in flow friction

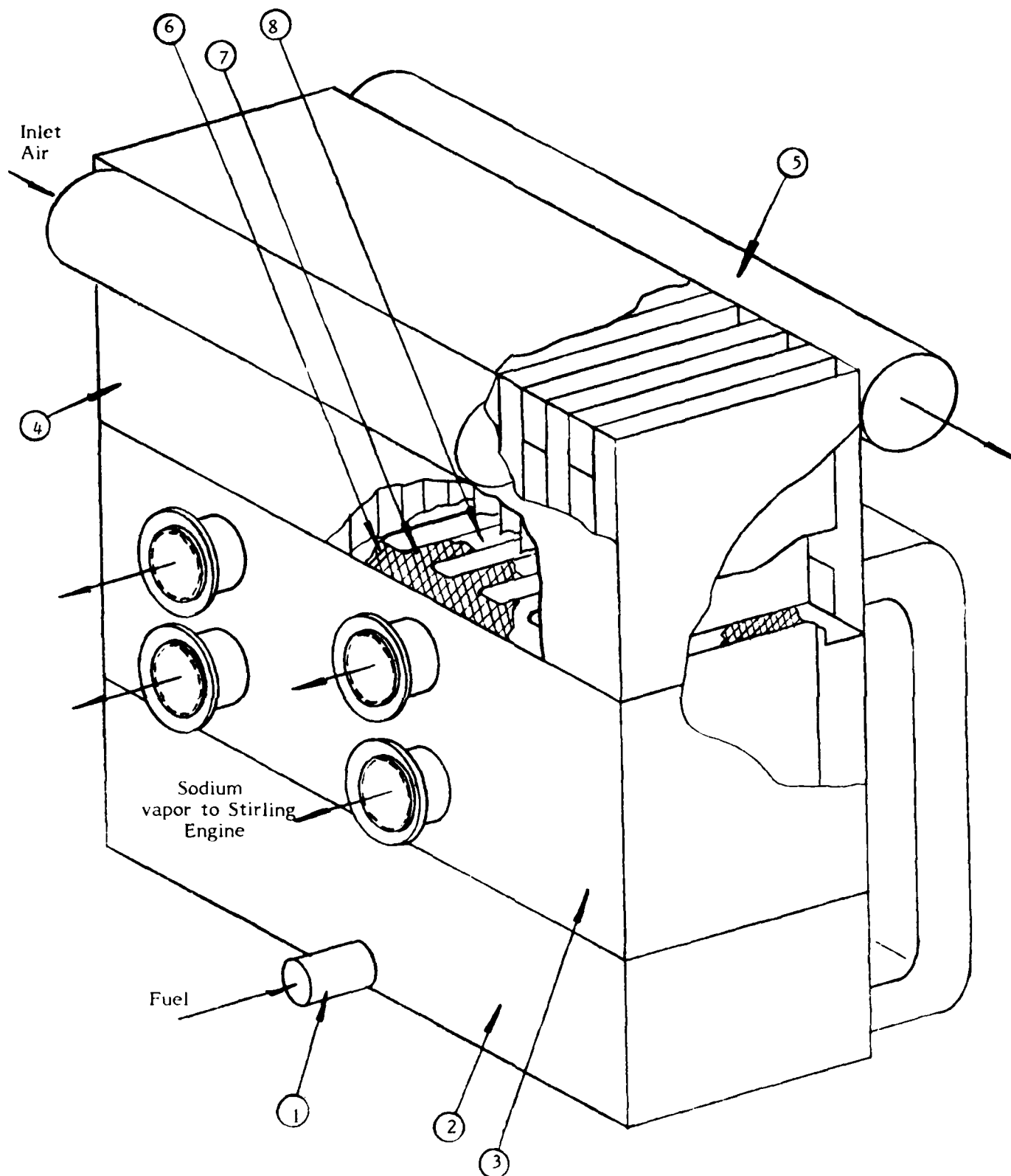


Figure 1 - External Heating System Schematic Illustration

- (1) Fuel atomizing nozzle (2) Combustion chamber (3) Heat exchanger/evaporator
 (4) Air preheater (5) Exhaust (6) Supporting wire mesh (7) Fine gauze wick
 (8) Evaporator fin

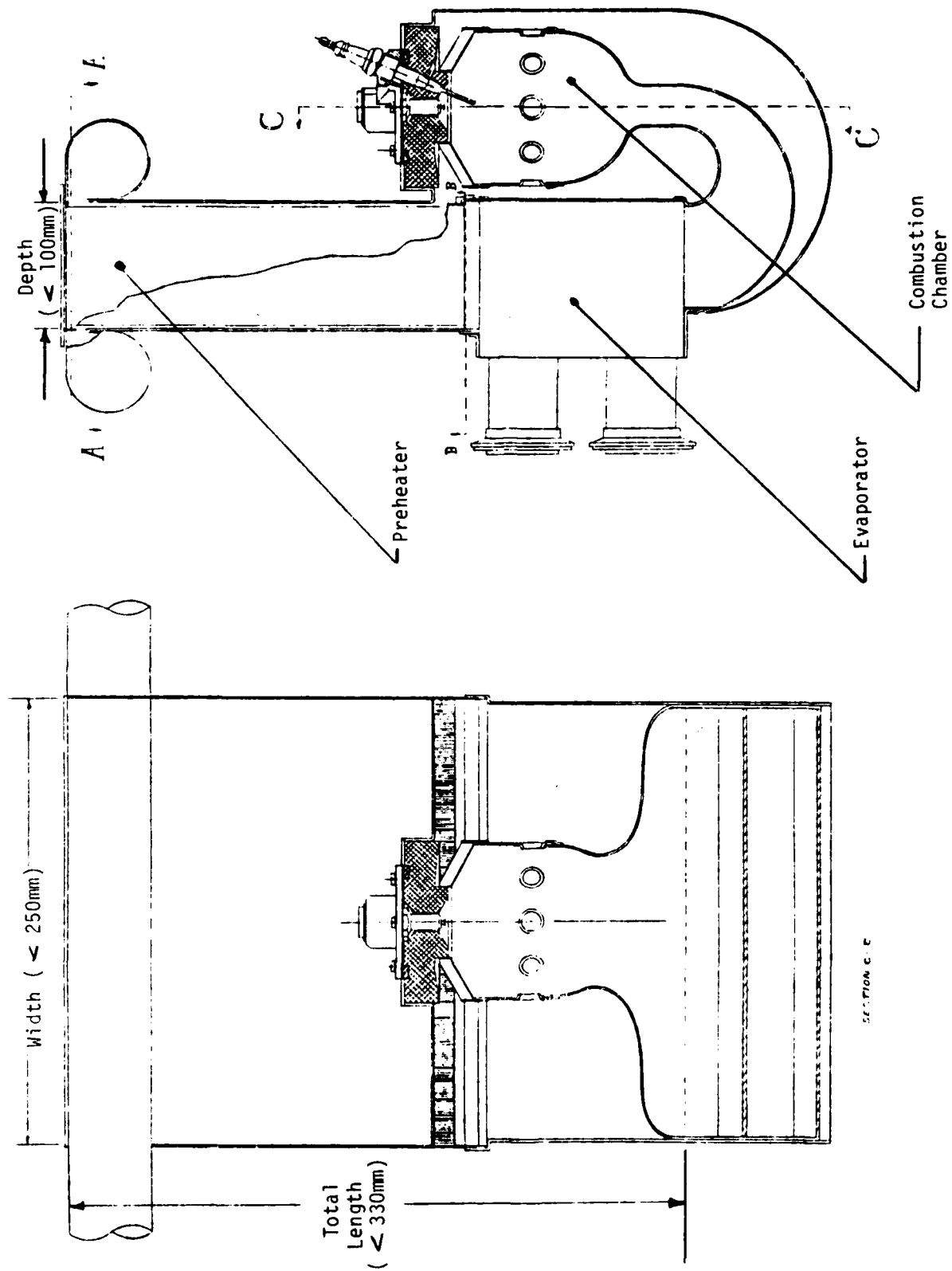


Figure 2
Packaging Requirements of the EHS

power loss, as shown in Table 1. The narrowest gap deemed practical was 1.0 mm.

2. SYSTEM ANALYSIS AND OPTIMIZATION

The geometrical parameters of the recuperator (or preheater) and heat exchanger alone determine the performance of the EHS provided that proper mixing and residence time can be achieved in the combustion chamber. Since an existing design of proven satisfactory performance was specified for the burner, the combustion chamber design was decoupled from the system analysis and optimization.

a. Description of the System Analysis Code

The purpose of the analysis and simulation code was to determine the EHS efficiency and the effect on flow losses and cold start fuel consumption based on the geometric parameters of the recuperator and heat exchanger.

Aerodynamic and heat transfer models were employed to define the design parameters based upon the heat transfer between the exhaust and intake air in the recuperator, the combustion characteristics of the fuel and burner, and the heat transfer from the flue gas to the heat pipe evaporator [5] [6].

In heat transfer calculations, the temperature dependent properties of the air and flue gas were taken into consideration [7] and therefore, a finite differences numerical scheme was used to solve the energy equations. Furthermore, in calculation of the flame temperature and heat exchanger performance, the dissociation of the flue gas was taken into consideration.

Table 1

Comparison of a Single Path and Multi Parallel Paths Heat Exchangers of Equal Total Heat Transfer Area

	<u>Single path of length $n\ell$</u>	<u>n parallel paths of length ℓ</u>
Volumetric flow	\dot{V}	$\dot{V}' = \dot{V}$
Heat transfer area	A	$A' = A$
Cross sectional (flow) area	S	$S' = nS$
Flow speed	$u = \dot{V}/S$	$u' = \frac{\dot{V}'}{S'} = \frac{V}{nS} = \frac{u}{n}$
Reynolds number	$Re = \frac{\rho u d_h}{\mu}$	$Re' = \frac{\rho u' d_h}{\mu} = \frac{\rho (u/n) d_h}{\mu} = \frac{Re}{n}$
Nusselt number	Nu	$Nu' = Nu$
Prandtl number	Pr	$Pr' = Pr$
NTU	$\Lambda = \frac{Nu}{RePr} \frac{A}{S}$	$\Lambda' = \frac{Nu'}{Re'Pr'} \frac{A'}{S'} = \frac{Nu}{(Re/n)Pr} \frac{A}{nS} = \Lambda$
Pressure drop	$\Delta p = \frac{48}{Re} \rho u^2 \frac{(n\ell)}{d_h}$	$\Delta p' = \frac{48}{(Re/n)} \rho \left(\frac{u}{n}\right)^2 \frac{\ell}{d_h} = \frac{\Delta p}{n^2}$
Flow friction power	$P_f = \dot{V} \Delta p$	$P_f' = \dot{V}' \Delta p' = \dot{V} \left(\frac{\Delta p}{n}\right) = P_f/n$

This effect was neglected in the analysis of the recuperator since the temperatures are sufficiently low.

Since the total laminar pressure drop in the heat exchangers was expected to be less than 50 cm of water it was deemed unnecessary to take into account the variable fluid properties in the flow direction. The pressure drop was determined for each component separately, based on Poiseuille flow at the average temperature prevalent in that component. These average temperatures were calculated by numerical integration.

The code was designed to accommodate any fuel (atomic hydrogen to carbon ratios between 0.25 and 4.0) and equivalence ratios ranging from 1.0 to 1.4.

The governing equations for the preheater and heat exchanger/evaporator heat transfer analyses are included in Appendix B. A sample computer run is included in Appendix C.

b. Results of the System Analysis and Optimization

In order to investigate the influence of the ratio of the evaporator area to the recuperator area (with a constant sum thereof) a series of simulations was made with the following geometric parameters unchanged; fin/plate depth, number of gaps and gap width in both the evaporator and recuperator, and the sum of the lengths of the evaporator and recuperator.

The results are summarized in Figures 3 and 4 showing, respectively, the effect of the area ratio on the efficiency and the cold start fuel consumption. The area ratio is defined as the ratio of recuperator area to heat exchanger/evaporator area. The cold start fuel consumption decreases with an increase of the area ratio, and efficiency exhibits a maximum at an

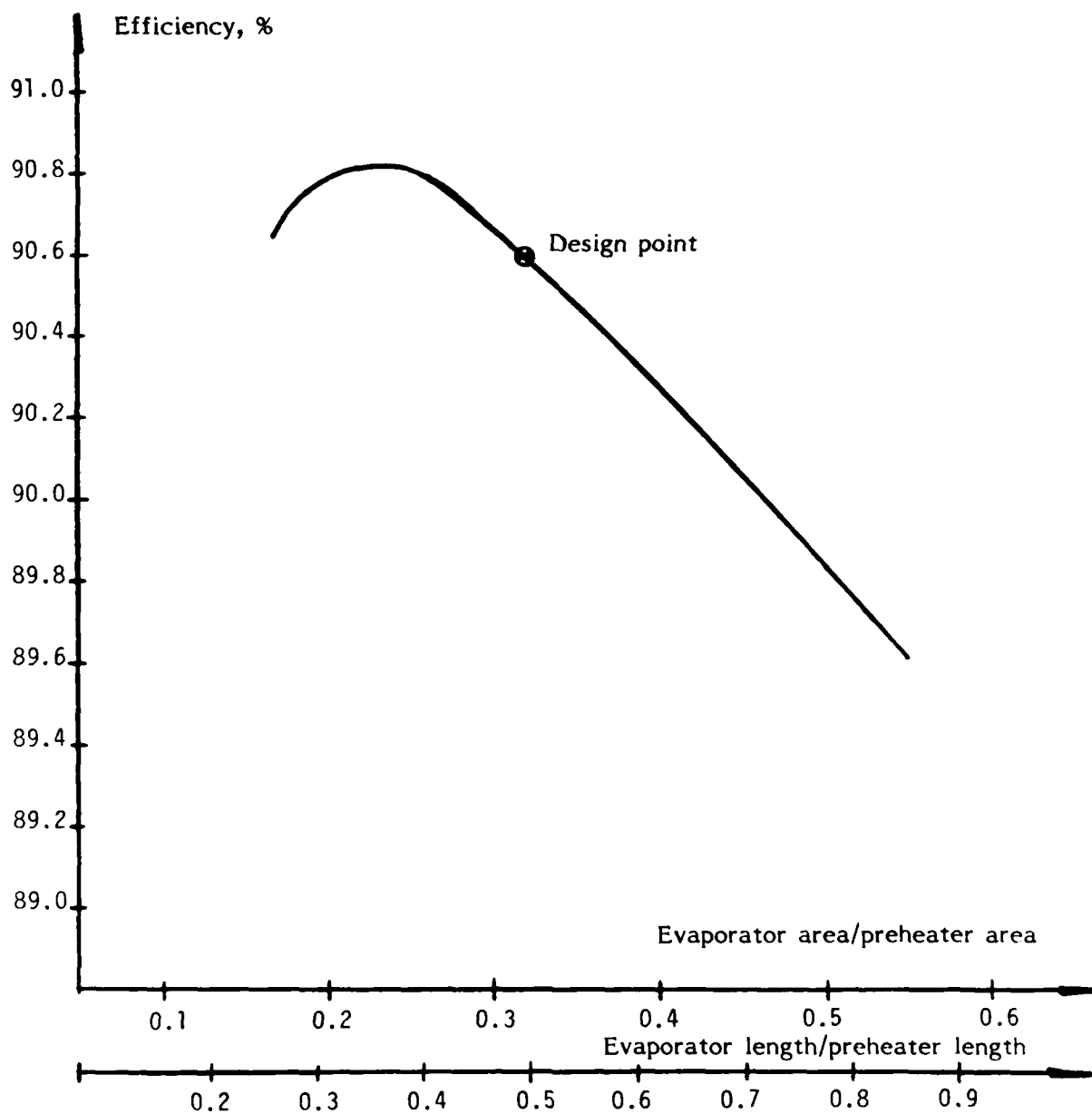


Figure 3

Effect of Area Ratio on EHS Efficiency

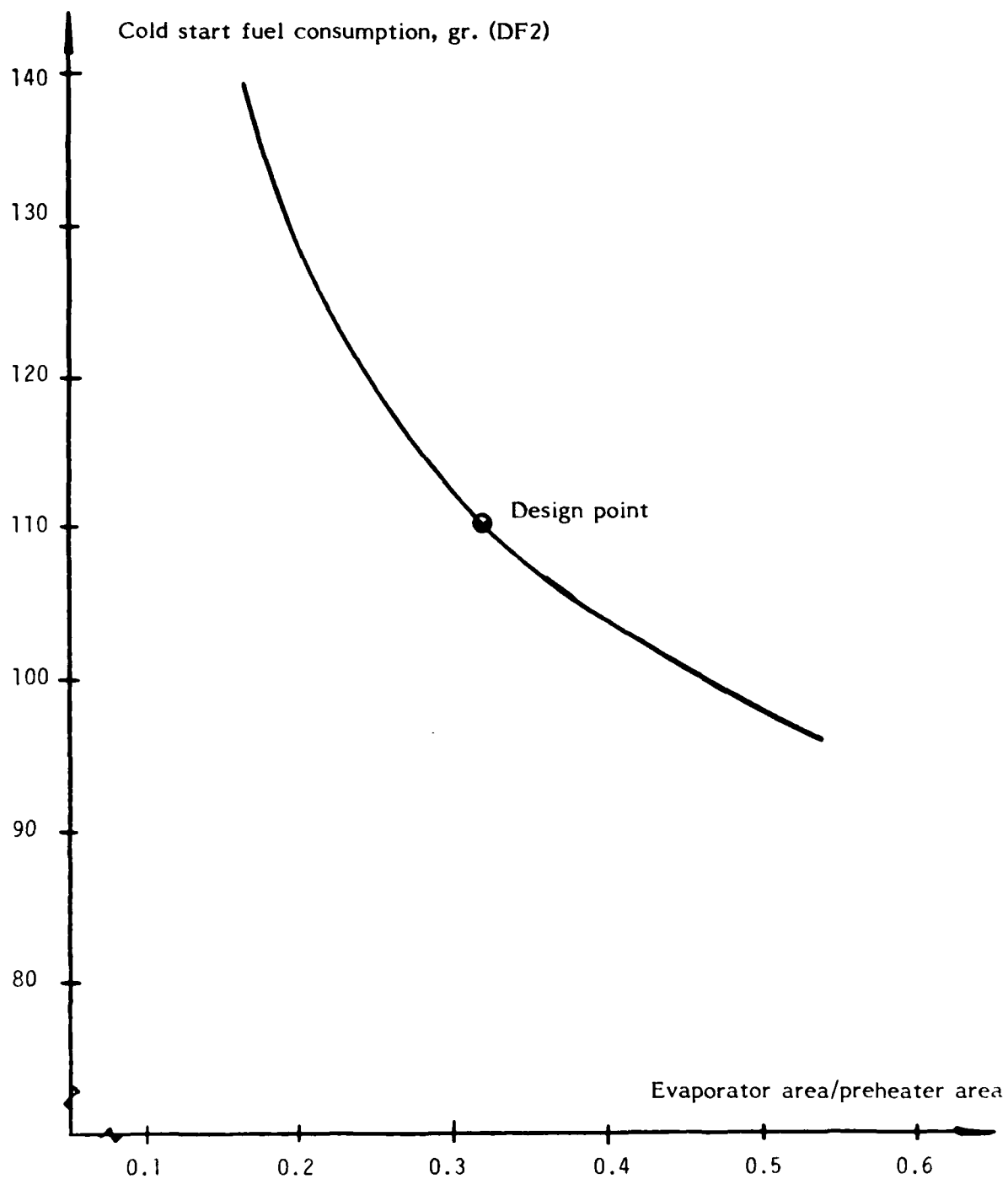


Figure 4

Effect of Area Ratio on EHS Cold Start Fuel Consumption

area ratio value of approximately 0.25. A design point of 0.32 was chosen to account for possible deviation of the analytical model from reality and to allow sufficient interface space. That area ratio was held constant for the rest of the investigation.

The effect of total heat transfer area at a constant ratio of heat transfer area to cross sectional area was investigated by a series of simulations with increasing depth of the evaporator fins and recuperator plates maintaining all other geometric parameters constant. The results are summarized in Figures 5, 6, and 7, showing respectively, the effect of the total heat transfer area on the efficiency, flow losses and cold start fuel consumption. A design point at the total area of 4.235 m² corresponding to a fin/plate depth of 70 mm was selected as a favorable compromise between efficiency and flow losses on one hand and cold start fuel consumption (size, weight, and cost) on the other hand.

It should be noted that the efficiency and cold start fuel consumption in Figures 3 and 4 differ from the values in Figures 5 and 7. This is due to the iterative procedure used to determine first the design point with regard to area ratio, then the design point with regard to total heat transfer area. The final value of total area is larger than the value used to determine area ratio.

Finally, the sensitivity of the performance to the gap width was investigated by a series of simulations with varying gap width. The number of gaps for each simulation was determined based on the gap width so that the total width of the heat exchangers was maintained constant at 250 mm. The results of this investigation, summarized in Figures 8 and 9, shows as expected, that increasing the gap width has an adverse effect on the

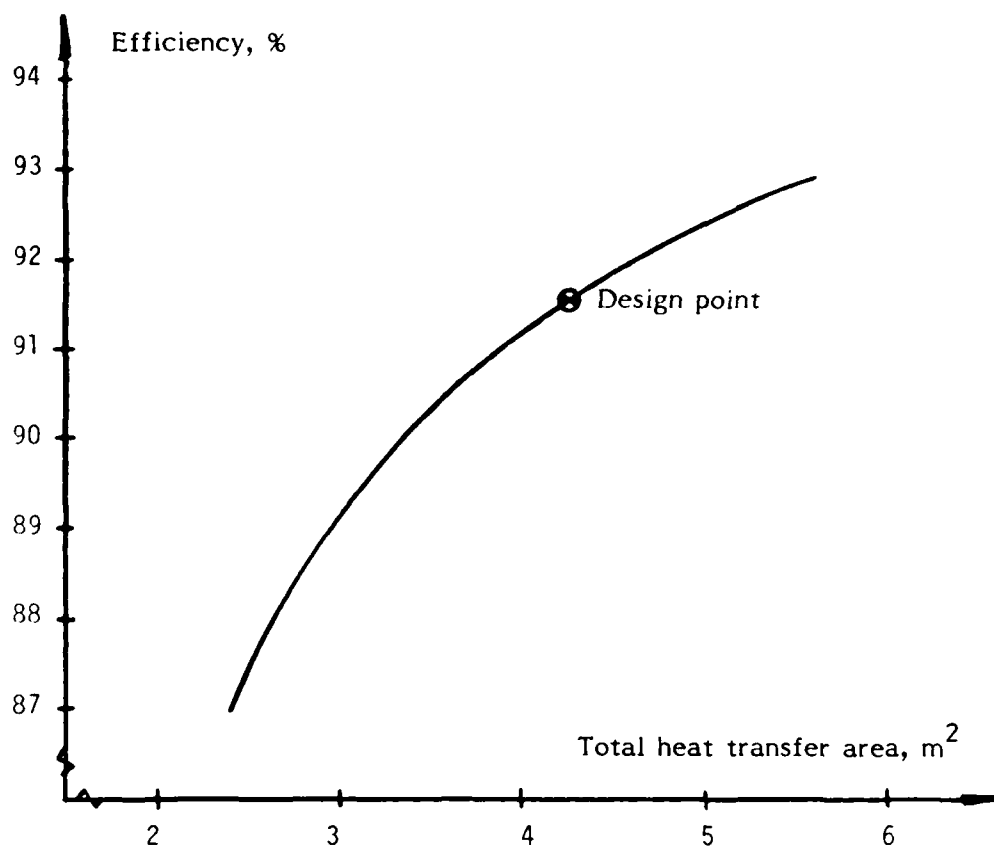


Figure 5

Effect of Total Heat Transfer Area on EHS Efficiency

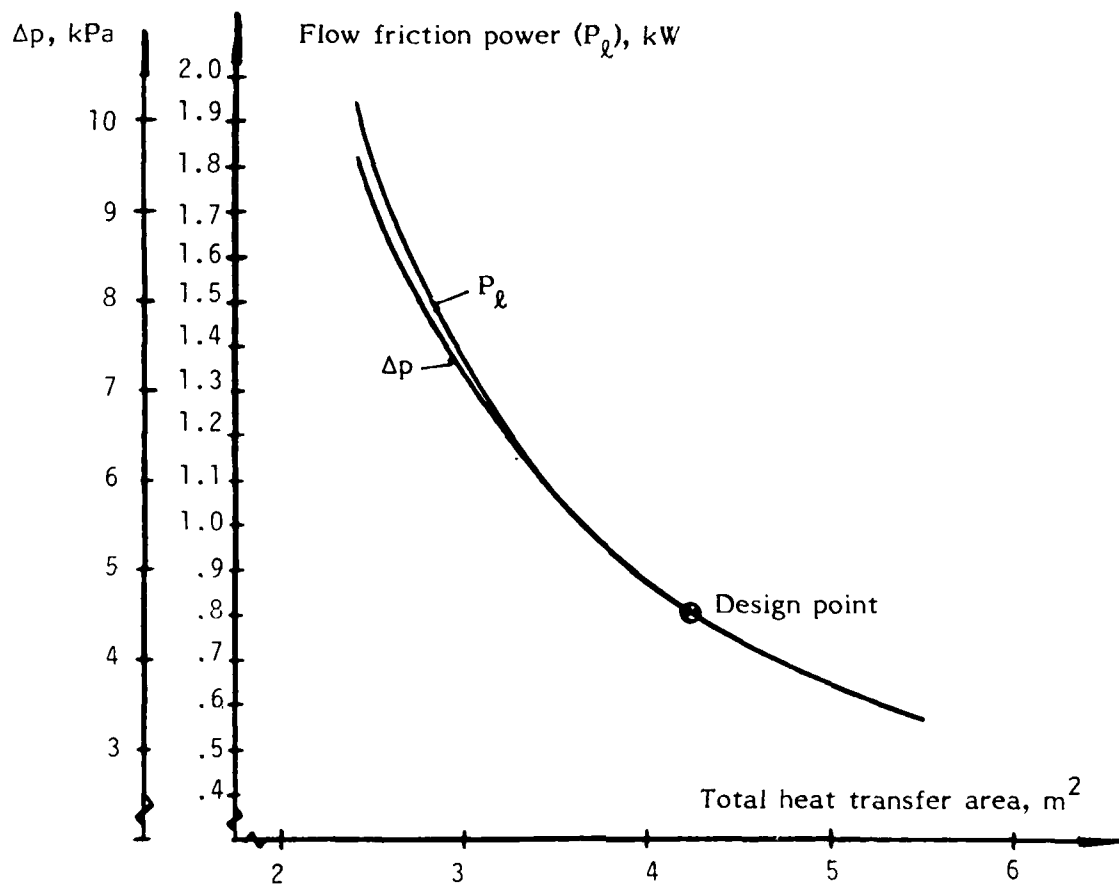


Figure 6

Effect of Total Heat Transfer Area on EHS Flow Friction Power

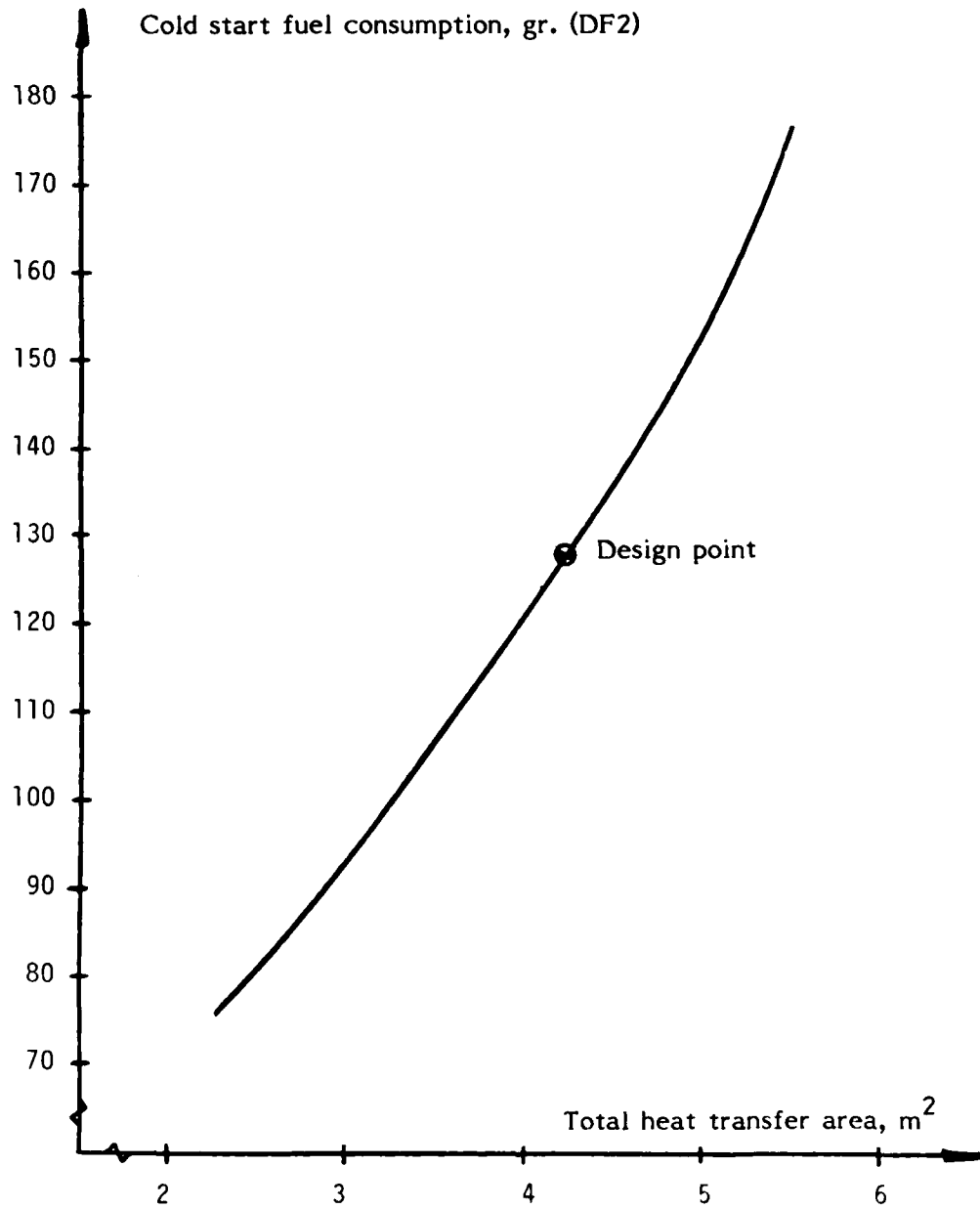


Figure 7

Effect of Total Heat Transfer Area on EHS Cold Start Fuel Consumption

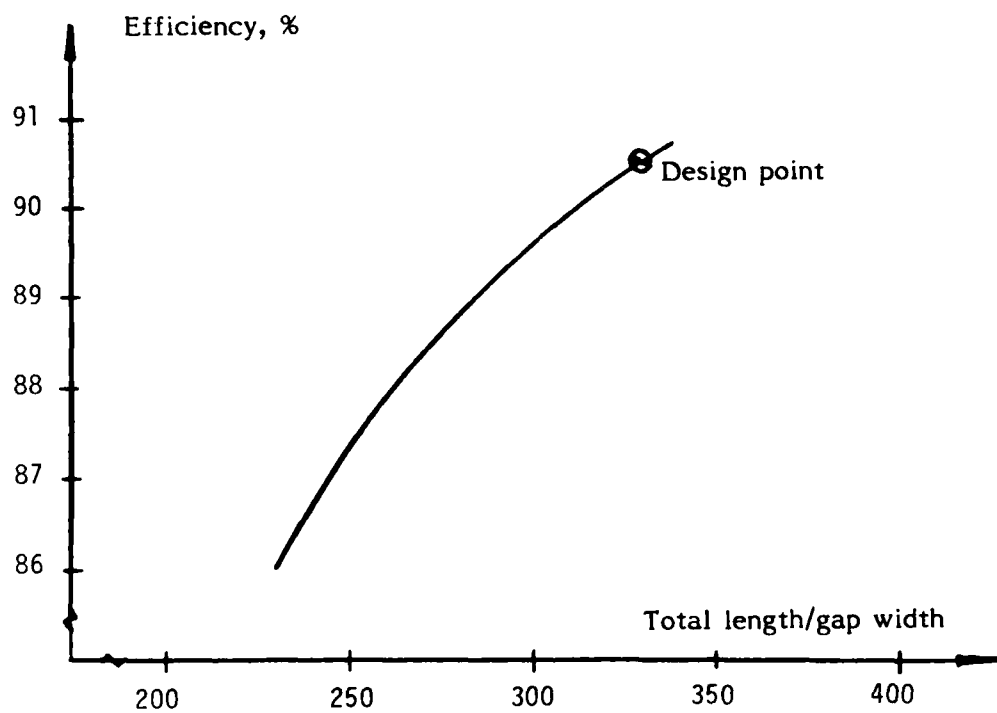


Figure 8

Effect of Gap Width on EHS Efficiency

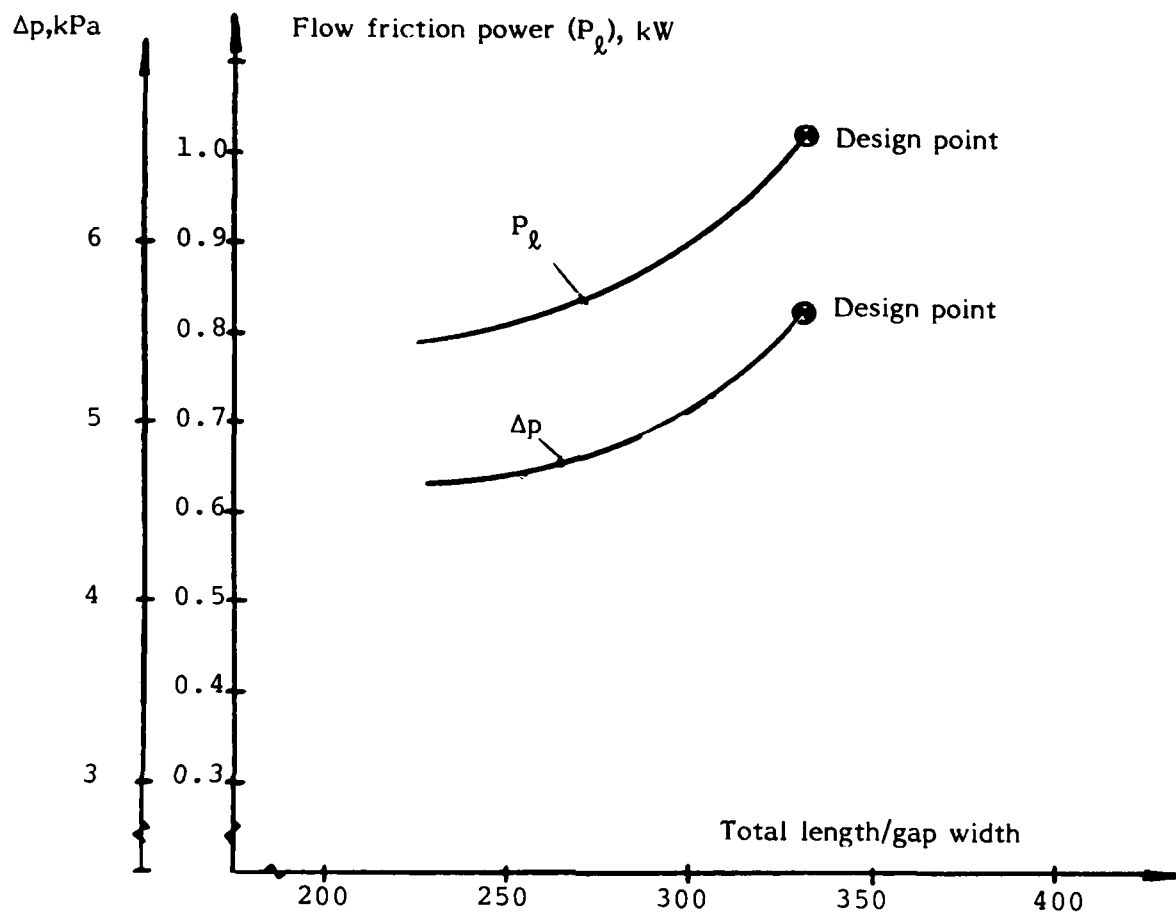


Figure 9

Effect of Gap Width on EHS Flow Friction Power

efficiency which is much more severe than the beneficial effect on flow losses. Consequently a gap width of 1.0 mm was retained as the design point.

The entire investigation was performed at full load corresponding to DF2 fuel consumption of 2.67 grams/sec with an equivalence ratio of 1.25 (air/fuel ratio of 18:1), 4% atomizing air and no EGR. The material wall thickness was kept at 0.2 mm. The goals of this investigation were to establish preliminary design parameters, hence the effects of fouling and corrosion were not taken into consideration.

The performance at the above conditions with the selected geometric parameters is summarized in Table 2 and Figures 10a and 10b.

Table 2

STM4-120 EHS Performance Data

	Preheater		Evaporator
Geometric Data	Air Side	Flue Side	
Length, mm	220	220	110
Depth, mm	70	70	70
Gap width, mm	1.0	1.0	1.0
Number of gaps	104	104	67
Wall thickness, mm	0.2	0.2	0.2
<u>Temperature data</u>			
Average (bulk) temperatures, K	694	827	1370
<u>Fuel Data (DF2)</u>			
Atomic H/C ratio		1.804	
Specific lower heating value		10.179 cal./gr.	
<u>Operating Data</u>			
Equivalence ratio		1.25	
Atomizing air		4%	
Fuel consumption		2,67 gr./sec.	
Ambient temperature		301 K	
Heat pipe temperature		1085 K	
<u>Performance</u>			
Preheated air temperature		1034 K	
Flame temperature		2397 K	
Heat exchanger outlet temperature		1097 K	
Exhaust outlet temperature		498 K	
Heat output		104 kW	
EHS Efficiency		91.6%	
Cold start penalty		128.3 gr.	
Pressure drop		4.64 k Pa	
Flow losses		819 Watt	

Figure 10a

Steady State Temperature Profile in STM4-120 EHS

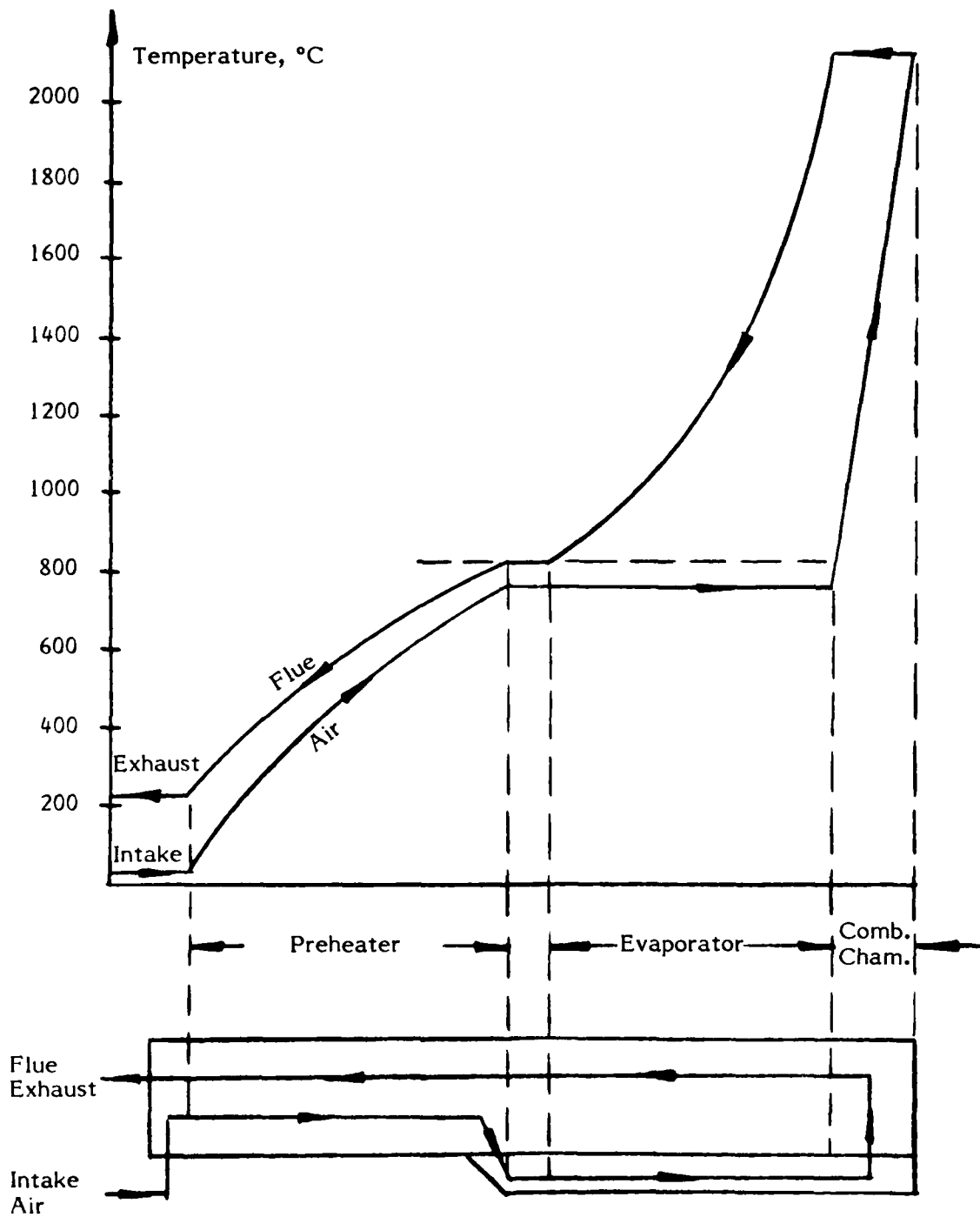


Figure 10b

Flow Path Through STM4-120 EHS

SECTION III

HEAT PIPE PRELIMINARY DESIGN

The conceptual Stirling powered electrical generator set includes the STM4-120 Energy Conversion Unit (ECU) coupled to the EHS through four heat pipe tubes with mechanical couplings that simultaneously supply the ECU with heat via sodium vapor and return the sodium condensate to the EHS.

In this section, a brief review of current heat pipe theory is presented, followed by a description of the EHS heat pipe configuration and the application of the theory to the particular design for the EHS.

1. Heat Pipe Theory

The theory of heat pipes is well documented in the literature, hence only a brief review of current theory is presented to provide a basis for the hydrodynamic and thermal design of the EHS heat pipe. Parts of this section are excerpted from "Theory and Design of Variable Conductance Heat Pipes," by D.B. Marcus, NASA Report Number CR-2018. A listing of other pertinent references is included in that report.

a. Hydrodynamics

Because a heat pipe involves the circulation of a working fluid, certain pressure drops arise. In general, there will be viscous losses due to liquid flow in the wick or capillary structure, and viscous and inertial losses due to vapor flow in the core. In addition, there may be body forces that either aid or hinder circulation (e.g. acceleration fields due to

etc.). For steady state operation of a heat pipe, a pressure head equal to the sum of these losses must be supplied by the capillary in the wick. This yields the following steady state pressure balance, which must be satisfied between all points along the heat pipe.

$$\Delta P_c = \Delta P_\ell + \Delta P_v \pm \Delta P_b \quad (1)$$

$$\left[\begin{array}{c} \text{net} \\ \text{capillary} \\ \text{head} \end{array} \right] = \left[\begin{array}{c} \text{liquid} \\ \text{pressure} \\ \text{drop} \end{array} \right] + \left[\begin{array}{c} \text{vapor} \\ \text{pressure} \\ \text{drop} \end{array} \right] \pm \left[\begin{array}{c} \text{body force} \\ \text{head} \\ \text{(if any)} \end{array} \right]$$

(1) Capillary Head

Of the terms in Eq. 1, the liquid and vapor pressure drops are functions of the circulation rate and increase with the heat transfer load on the device, while the body force term is usually independent of the load. Thus, to satisfy Eq. 1, the capillary head must also increase with load in such a way as to match the losses incurred.

The capillary head in a saturated heat pipe wick arises as a dynamic phenomenon. It is due to the existence of a pressure difference across a curved liquid-vapor interface which is given by:

$$\Delta P_i = \sigma \left(\frac{1}{R_1} + \frac{1}{R_2} \right) \quad (2)$$

where ΔP_i = Interfacial pressure difference

σ = Surface Tension

R_1, R_2 = Two orthogonal radii of curvature of the interface

This pressure difference, which for concave menisci results in a depression of the liquid pressure with respect to the vapor, exists all along the heat pipe wick. In order to obtain a net capillary head, it is necessary for it to be greater at the evaporator than at the condenser. In a heat pipe under load, this is exactly what occurs due to changes in the interface curvatures. Vaporization of the liquid in the evaporator causes the menisci to recede into the wick resulting in a decrease in the radii of curvature, while condensation in the condenser has the opposite effect. Therefore, capillary pressure is not constant. Capillary pumping is a passive phenomenon which automatically adjusts to meet the flow requirements, within limits.

The extremes of the interfacial pressure difference, which can be generated along the wick depend on the wick geometry and the wetting angle between the liquid and wick material. For the EHS application, the wick was specified to be stainless steel wire mesh, based on previous experience. For this type of wick, the maximum capillary pressure becomes:

$$P_{c \max} = \frac{2\sigma}{r_c} \quad (3)$$

where r_c = effective capillary radius, $= \frac{w + d}{2}$

w = wire spacing

d = wire diameter

(2) Liquid Pressure Drop

Liquid flow in heat pipes is generally characterized by very

low velocities and Reynolds numbers. Consequently, inertial effects can be neglected for steady state operation and the flow losses attributed only to viscous shear.

The pressure drop in wire mesh wicks can be expressed as a form of Darcy's Law for flow in porous media, which is usually expressed in terms of a permeability - K , a measure of the wick flow resistance.

$$\frac{dP_{\ell}}{dx} = \frac{\mu_{\ell} \dot{m}_{\ell}(x)}{K A_w \rho_{\ell}} \quad (4)$$

where μ_{ℓ} = liquid viscosity
 ρ_{ℓ} = liquid density
 $\dot{m}_{\ell}(x)$ = local axial mass flow rate
 A_w = wick cross-sectional area
 K = wick permeability

Experimental data on tightly wrapped wire mesh wicks have been correlated by a modified Blake-Kozeny equation:

$$K = \frac{d^2 \epsilon^3}{122 (1 - \epsilon)^2} \quad (5)$$

In Eq. 5, d is the wire diameter and ϵ can be calculated by the

equation:

$$\epsilon = 1 - \pi/4 \text{ SNd} \quad (6)$$

where N = mesh number

S = crimping factor ≈ 1.05

(3) Vapor Pressure Drop

The vapor pressure drop in heat pipes is often considerably more difficult to calculate than that in the liquid, for in addition to viscous shear, the analysis must account for momentum effects and perhaps turbulent flow and compressibility. Complicating this analysis is the fact that mass addition in the evaporator and mass removal in the condenser can significantly alter the velocity profiles and hence, the local pressure gradient.

From conservation of momentum, the vapor pressure drop can be expressed as follows:

$$\frac{dP_v}{dx} = \frac{-(f_v Re_v) \mu_v \dot{m}_v}{2 A_v r_v^2 \rho_v} - \beta \frac{2 \dot{m}_v}{A_v^2 \rho_v} \frac{d\dot{m}_v}{dx} \quad (7)$$

Here, the first group represents the pressure drop due to viscous shear and the second group represents the pressure drop due to inertial effects, where f_v is the frictional drag coefficient and β is defined by the

equation:

$$\beta = \frac{\rho_v^2 A_v}{\dot{m}_v^2} \int_{A_v} V^2 dA \quad (8)$$

Equation 8 accounts for the effects of changes in vapor velocity across the section of consideration.

(4) Body Force Head

The last term in the pressure balance equation is the pressure head due to body forces acting on the working fluid. In the EHS heat pipe, the only body force that arises is due to the acceleration of gravity. Since the density of the vapor is very much lower than that of the liquid, the body forces on the vapor can be neglected. The pressure head due to the gravitational field is expressed by the equation:

$$\Delta P_g = \int \frac{dP_g}{dz} = \pm \int \rho_l g \cos \theta dz \quad (9)$$

where ΔP_g = component of the hydrostatic head in the direction of liquid flow

g = acceleration of gravity

θ = angle of the liquid flow axis with respect to the direction of gravitational acceleration

dz = elemental length

(5) Capillary Pumping Limit

The fact that there exists a maximum capillary head for any wick-fluid combination results in a hydrodynamic limit on heat pipe capacity. As mentioned previously, the capillary head must increase with the liquid and vapor pressure drops as the heat load increases. Since there exists a limit on the capillary head there must also exist a corresponding limit on the heat load if the pressure balance criterion is to be satisfied. This defines the capillary pumping limit, expressed by the following inequality:

$$\Delta P_{c_{\max}} - \Delta P_g \geq \Delta P_l + \Delta P_v \quad (10)$$

(6) Entrainment Limit

A phenomenon which can effect the capillary pumping limit, but was not included in Eq. 10, is liquid entrainment in the vapor. In a heat pipe, the vapor and liquid generally flow in different, often opposite, directions. Since they are in contact at the wick surface, this sets up a mutual drag at the interface. If the relative velocity between the liquid and the vapor becomes too great, the interface becomes unstable and droplets of liquid will be torn from the wick and entrained in the vapor. Since this liquid never reaches the evaporator, it cannot contribute to the heat transferred by the heat pipe. However, it does contribute to the liquid flow loss. Thus, the maximum axial heat transfer in the heat pipe is no longer equal to the maximum fluid circulation rate times the latent heat of vaporization, but some lower value which defines the entrainment limit.

The conditions leading to entrainment are expressed in terms of the ratio of vapor inertial forces to liquid surface tension forces, called the Weber number:

$$W_e = \frac{\rho_v \bar{V}^2 z}{\sigma} \quad (11)$$

where ρ_v = vapor density
 \bar{V} = average vapor velocity
 σ = liquid surface tension
 z = characteristic dimension associated with liquid surface

Limited experimental data with screen wicks indicate that a Weber number of unity represents the entrainment condition when the characteristic dimension, z , is set approximately to the screen wire diameter [8].

When the Weber number is set equal to unity, the limiting axial heat flux corresponding to incipient entrainment is given by:

$$\frac{Q_{e_{\max}}}{A_v} = \left[\frac{\rho_v \sigma \lambda^2}{z} \right]^{\frac{1}{2}} \quad (12)$$

where $Q_{e_{\max}}$ = Maximum heat flux for incipient entrainment
 A_v = Vapor core flow area
 λ = Latent heat of vaporization

(7) Sonic Limitation

It can be shown analytically [9] that there is a correspondence between constant area flow in a heat pipe with mass addition (evaporator) and removal (condenser) and constant mass flow in a converging-diverging nozzle. The end of the evaporator corresponds to the throat of the nozzle. Consequently, just as there is a sonic limitation on the flow velocity through a nozzle throat, there is a similar limit on the flow velocity at the heat pipe evaporator exit. For a given exit temperature and working fluid, this choked flow condition is a fundamental limitation on the axial heat transfer flux capacity of the heat pipe.

The sonic limit is calculated by setting the vapor flow velocity equal to the sonic velocity in the continuity equation and multiplying by the latent heat of vaporization as follows:

$$\frac{Q_{s_{\max}}}{A_v} = \lambda \rho_v V_s \quad (13)$$

where $Q_{s_{\max}}$ = axial heat flux at Mach 1 conditions
 V_s = sonic velocity of the vapor

b. Heat Transfer

The fluid circulation phenomenon discussed in the previous sections arise as a result of heat transfer into the heat pipe at the evaporator and out of it at the condenser. In most heat pipes this heat must be transferred through the walls and saturated wick. Generally, these

processes are the major source of temperature drop in the heat pipe. Temperature drops also arise due to vapor flow losses along the heat pipe and to non-equilibrium at the liquid-vapor interfaces.

(1) Boiling Limitation

The fact that heat is transferred into the heat pipe through the wick gives rise to another limit on heat pipe capacity. Frequently, liquid is vaporized only at the wick surface as a result of heat conducted through the wick. However, the vapor at the wick surface is thermodynamically saturated, hence the fluid within the wick is superheated by virtue of the curvature of the menisci and the temperature gradient in the saturated wick. The greatest superheat occurs at the interface of the wick and wall. If this superheat becomes too large (it increases with the heat transfer rate), the fluid will begin to boil within the wick. This results in evaporator dryout due to a reduction in liquid flow area in the wick caused by nucleation.

Further discussion of boiling limitation is referred to the literature, since the heat flux was specified to be a value experimentally proven to be within the boiling limitation of the EHS evaporator configuration.

(2) Heat Pipe Temperature Characteristics

Generally, heat pipe temperature characteristics are evaluated at full load, since the associated gradients are at a maximum under these conditions. The temperature drops associated with heat pipes occur in the evaporator wall, the saturated wick, and the condenser wall due

to conduction. There is an additional, generally much smaller, temperature drop associated with the vapor pressure drop between the evaporator and the condenser due to vapor flow resistance.

(a) Temperature Drop Across the Evaporator Wall

The temperature of the outer wall of the evaporator is essentially constant at 1085 K (812°C). The temperature drop due to conduction across the wall can be expressed by the following equation:

$$\frac{\dot{Q}}{A} = k \frac{dT}{dx} \quad (14)$$

(b) Temperature Drop Across the Saturated Wick

The temperature drop across the saturated wick can be evaluated using Eq. 14. However, the thermal conductivity must be replaced by an effective conductivity of the wick/liquid combination. The effective conductivity, k_{eff} , for saturated screen wicks is:

$$k_{eff} = \frac{k_l [(k_l + k_w) - (1 - \epsilon)(k_l - k_w)]}{[(k_l + k_w) + (1 - \epsilon)(k_l - k_w)]} \quad (15)$$

where k_l = Liquid Thermal Conductivity

k_w = Wick Thermal Conductivity

ϵ = Wick Porosity

(c) Temperature Drop Due to Vapor Flow Resistance

The temperature drop of the vapor due to flow resistance can be evaluated using the Clausius-Clapeyron equation:

$$\Delta T_v \approx \frac{T_v}{\rho_v \lambda} \Delta P_v \quad (16)$$

(d) Temperature Drop Across the Condenser Tubes

The condensers for the EHS heat pipe are the STM4-120 engine heaters. These condensers are simple tube bundles sized to optimize the heat transfer to, and flow resistance of, the engine working fluid. The temperature drop across the condenser tubes can be evaluated by modifying Eq. 14 to cylindrical coordinates. The resulting equation is:

$$\Delta T = \frac{\dot{Q}}{2\pi Lk} \ln \left(\frac{r_2}{r_1} \right) \quad (17)$$

2. Heat Exchanger/Evaporator Configuration

The STM4-120 Energy Conversion Unit (ECU) is coupled to the EHS through four heat pipe tubes with mechanical couplings that simultaneously supply the ECU with heat via sodium vapor and return the sodium condensate to the EHS. The heat pipe configuration is shown schematically in Figure 11. Liquid return is accomplished via gravity by locating the EHS heat exchanger below the ECU.

Tests conducted at STM on the mechanical couplings, Aeroquip Conoseals,

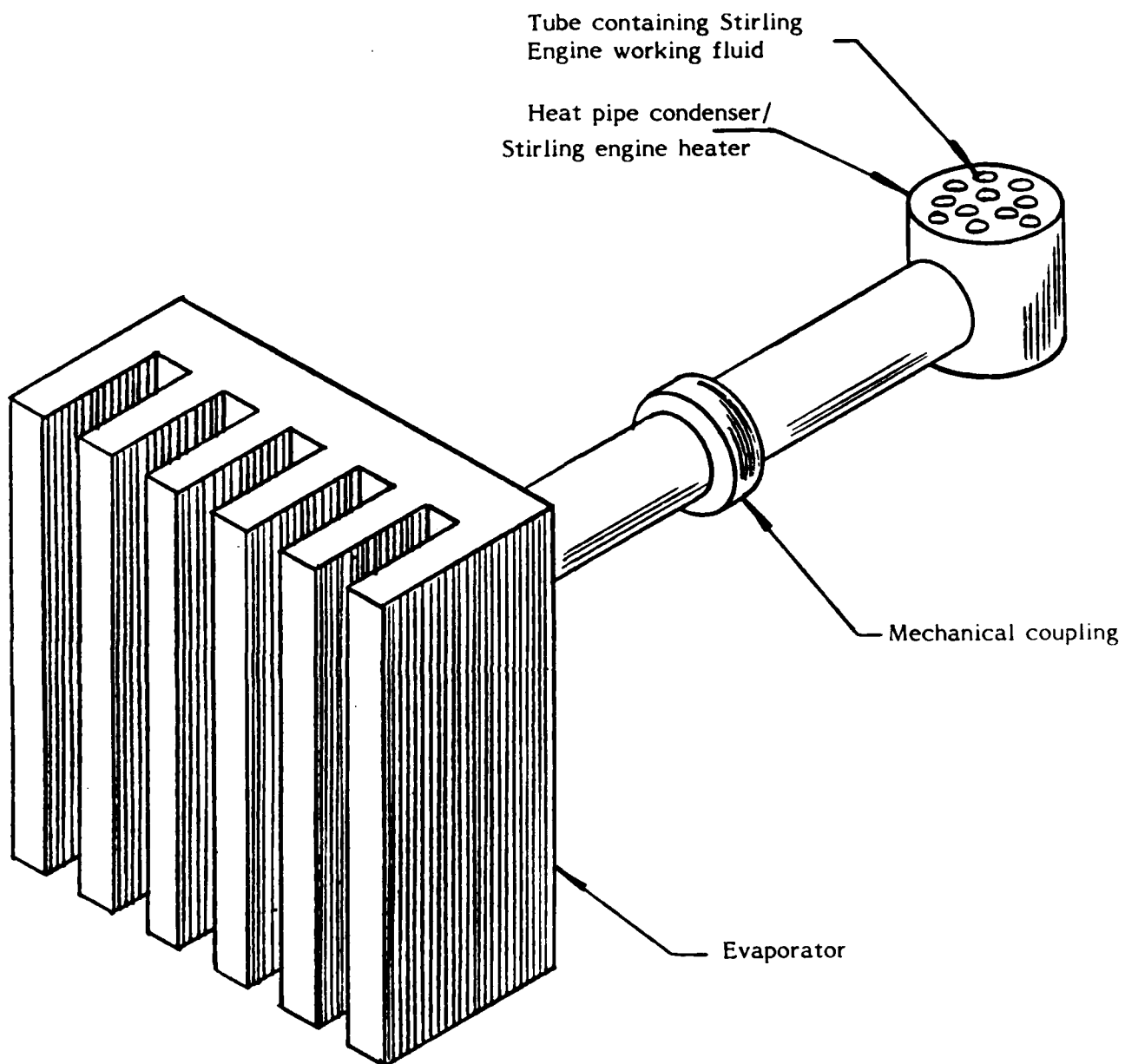


Figure 11

Schematic Representation of STM4-120 Heat Pipe

available from the Marman Division of Aeroquip, proved the functionality and durability of these seals in sodium heat pipe applications. One heat pipe with this coupling has operated for more than 1775 thermal cycles of heating to 800°C and cooling to 150°C. Another heat pipe with its wick capillary connection across this coupling has operated against gravity for more than 1000 hours. These tests are continuing [1]. An exploded view of a Conoseal joint is shown in Figure 12.

The EHS heat pipe configuration was examined as both buffered (moving front) and non-buffered designs. The buffered configuration permits easy start-up and temperature control but suffers from the fact that the sharp temperature gradients in the front create extremely high thermal stresses, especially in the engine heater. As the front passed through this heat exchanger, some of the tubes would be at 800°C and others would still be at ambient, resulting in unacceptably high stresses, and increasing the probability of heater tube failure.

In a non-buffered configuration, the entire heat pipe increases in temperature uniformly, eliminating the difficulties that result from thermal stresses. However, this configuration can experience start-up difficulties by condensing and freezing the sodium, drying out the evaporator before full fluid circulation can be established.

The EHS heat pipe fluid circulation was designed to return the maximum amount of sodium to the evaporator upon shut-down by wicking only the evaporator. This technique is only applicable if liquid return from the condenser can be accomplished without capillary pumping. In the EHS heat pipe, liquid return is accomplished via gravity.

Start-up is more readily accomplished since raising the temperature of

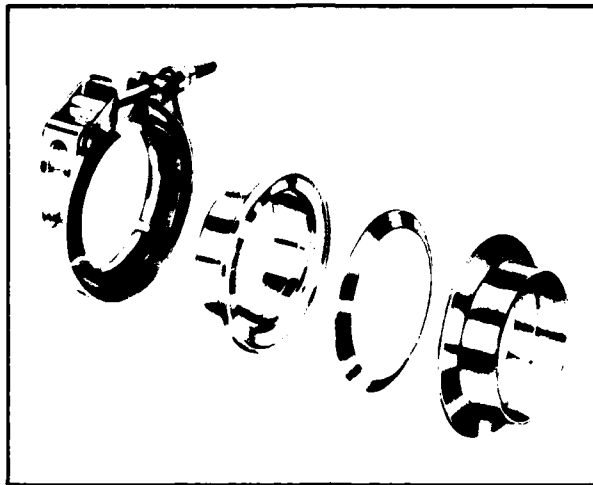


Figure 12

Medium Weight Conoseal Joint with T-bolt Quick Coupler

the working fluid occurs at the heat source, not at remote sections of the heat pipe which often require auxiliary heaters to melt the sodium to initiate fluid circulation.

The liquid collects in the bottom of the evaporator fins, where it contacts the wick lining the inside walls of the fins. The wick supplies liquid sodium over the entire inside surface of the evaporator through capillary pumping.

The evaporator configuration was based on the more difficult heat transfer from the flue gas to the evaporator wall, resulting in an average heat flux of 100 kW/m^2 . The maximum heat flux occurs at the bottom of the evaporator fins, where the flue gas enters the heat exchanger. The magnitude of the heat flux at this point is approximately 500 kW/m^2 . In experiments on sodium heat pipes at Philips and STM, this magnitude of heat flux was defined to be below the boiling limitation for sodium at 800°C , with commonly used wire mesh wicks. Once the configuration was established as compatible to the convective and radiative properties of the flue gas and the boiling properties of sodium, the design task was directed towards specification of a wick structure capable of maintaining an adequate supply of liquid sodium over the entire evaporator surface, i.e. satisfying the capillary pumping requirement, and providing structural support to the flat fins.

A coarse wire mesh was placed in the vapor path to provide structural support for the fins at a slight penalty in temperature uniformity due to vapor flow resistance, while simultaneously providing positive contact between the capillary wick and the evaporator wall. A schematic cross-section of the evaporator is shown in Figure 13.

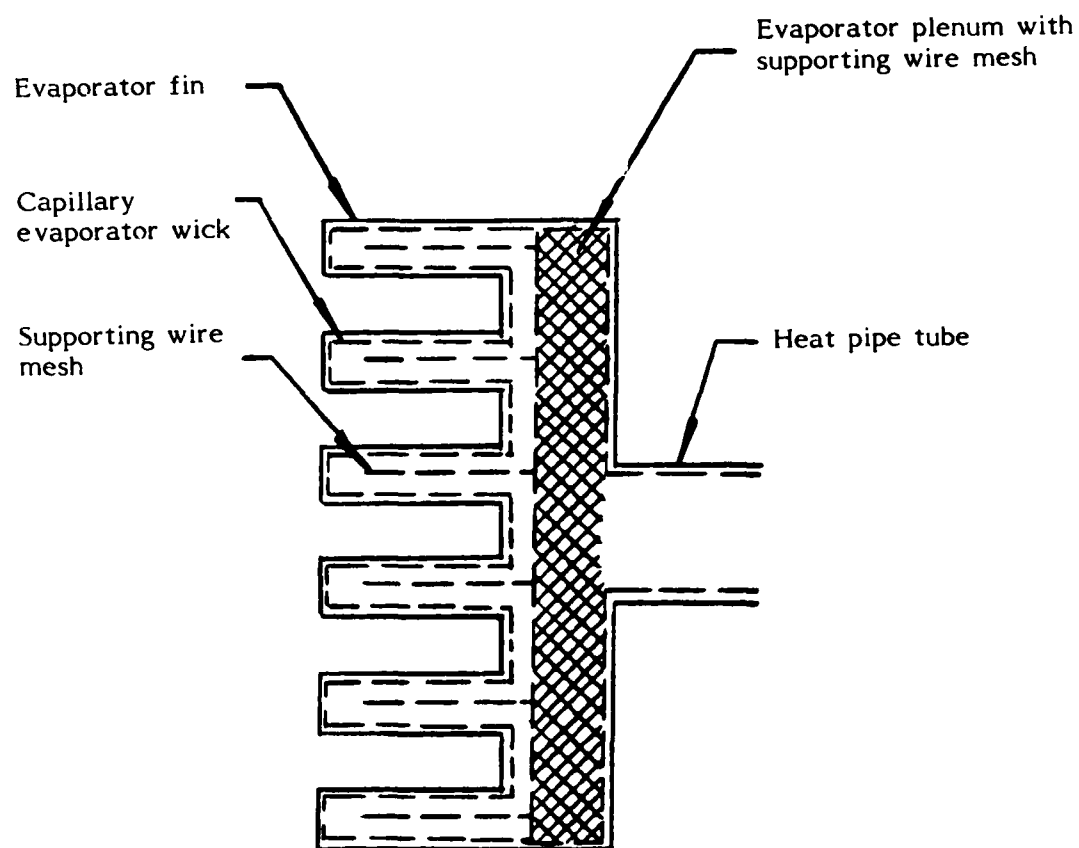


Figure 13

Schematic Representation of Heat Exchanger/Evaporator

3. Analysis of the Heat Exchanger/Evaporator

An analysis was conducted on the evaporator to evaluate capillary pressure as a function of position in a typical fin using various wick and support structures, while maintaining the external geometry defined in Table 2. The analysis was developed from basic heat pipe theory and empirical relations for flow properties of wire mesh wicks as previously summarized [10], [11], [12].

The most critical aspect of the evaporator design is maintaining sufficiently high capillary pressure in the wick to distribute the liquid throughout the fins. In addition, the coarse supporting mesh must withstand the structural load due to the pressure difference across the fin walls without significantly restricting the vapor flow out of the fin.

Sonic and entrainment limitations are a much lesser concern since the large number of fins, hence large vapor flow area results in vapor velocities well below a Mach Number of 0.2. This also simplifies the evaluation of the vapor pressure drop since the effects of the vapor compressibility can be neglected.

The heat flux from the flue gas to the evaporator varies according to the temperature distribution as shown in Figure 10. However, the evaporator analysis is greatly simplified by making the conservative assumption of constant heat flux. This assumption results in liquid flow only in the X (vertical) direction, and vapor flow only in the Y (horizontal) direction, essentially reducing the analysis to a one dimensional problem. The streamlines for liquid and vapor flow in both cases are shown in Figure 14.

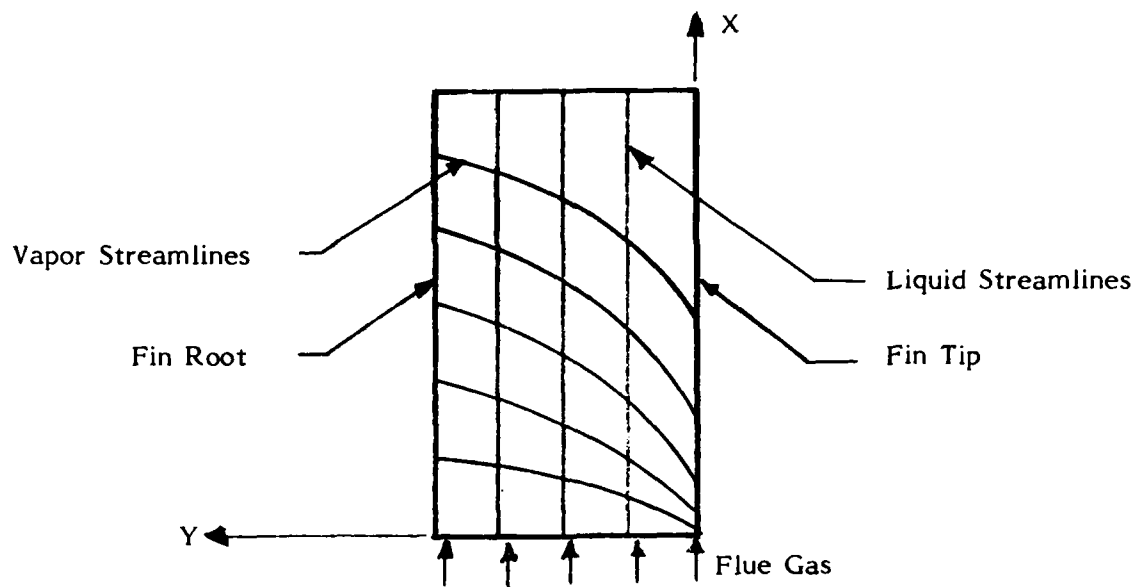


Figure 14a

Fluid Streamlines in a Typical Evaporator Fin with Varying Heat Flux

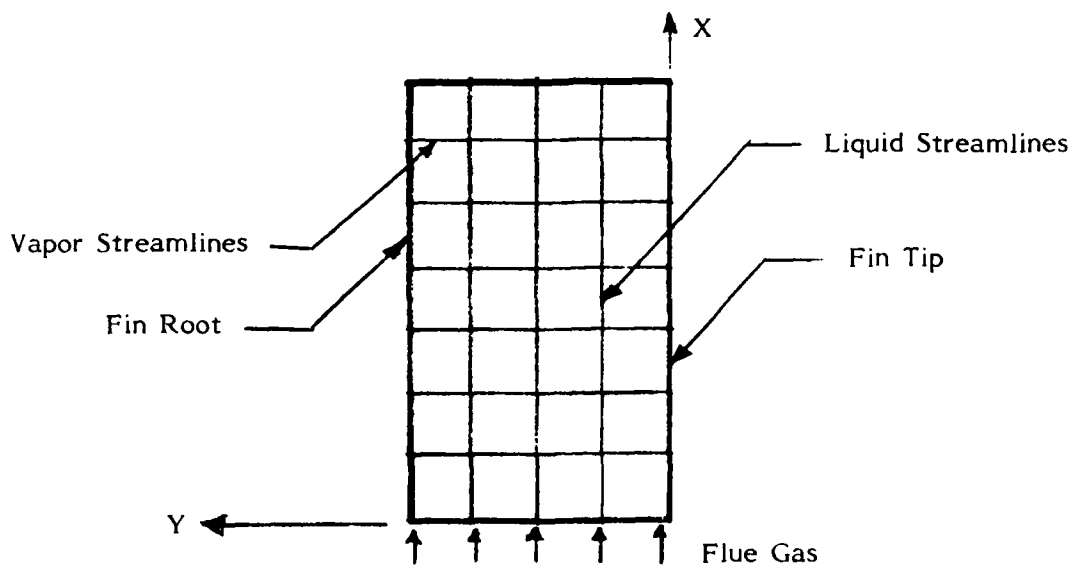


Figure 14b

Fluid Streamlines in a Typical Evaporator Fin with Constant Heat Flux

Application of Eq. 1 to the EHS evaporator results in the following equation:

$$\Delta P_c(x,y) = P_c(\text{ref}) + \Delta P_v + \Delta P_l + \Delta P_g \quad (18)$$

where $P_c(x,y)$ = capillary pressure at position (x,y)
 $P_c(\text{ref})$ = capillary pressure at a reference position $(x_{\text{ref}}, y_{\text{ref}})$
 ΔP_v = vapor pressure drop between (x,y) and $(x_{\text{ref}}, y_{\text{ref}})$
 ΔP_l = liquid pressure drop between (x,y) and $(x_{\text{ref}}, y_{\text{ref}})$
 ΔP_g = hydrostatic head (due to gravitational body force)

The reference position was defined to be at the bottom of the fins where it opens into the evaporator plenum since the capillary pressure must be at its minimum value. This conclusion can be deduced readily, since liquid and hydrostatic pressures here are defined to be zero, and clearly the vapor pressure must be at its smallest level in the fin at the root.

To satisfy Eq. 1 for the rest of the heat pipe, the minimum capillary pressure must be equal to the sum of the pressure drops in the rest of the heat pipe.

Vapor and liquid flow resistance are functions of the mesh geometry and fluid properties. Development of the liquid and vapor pressure drop equations 4 and 7, respectively, to the EHS finned evaporator application can be found in Appendix D. The results of the analysis are summarized in Figure 15.

Several simulations were conducted using various meshes fitting the geometric restrictions as noted in Table 2. Several wick configurations

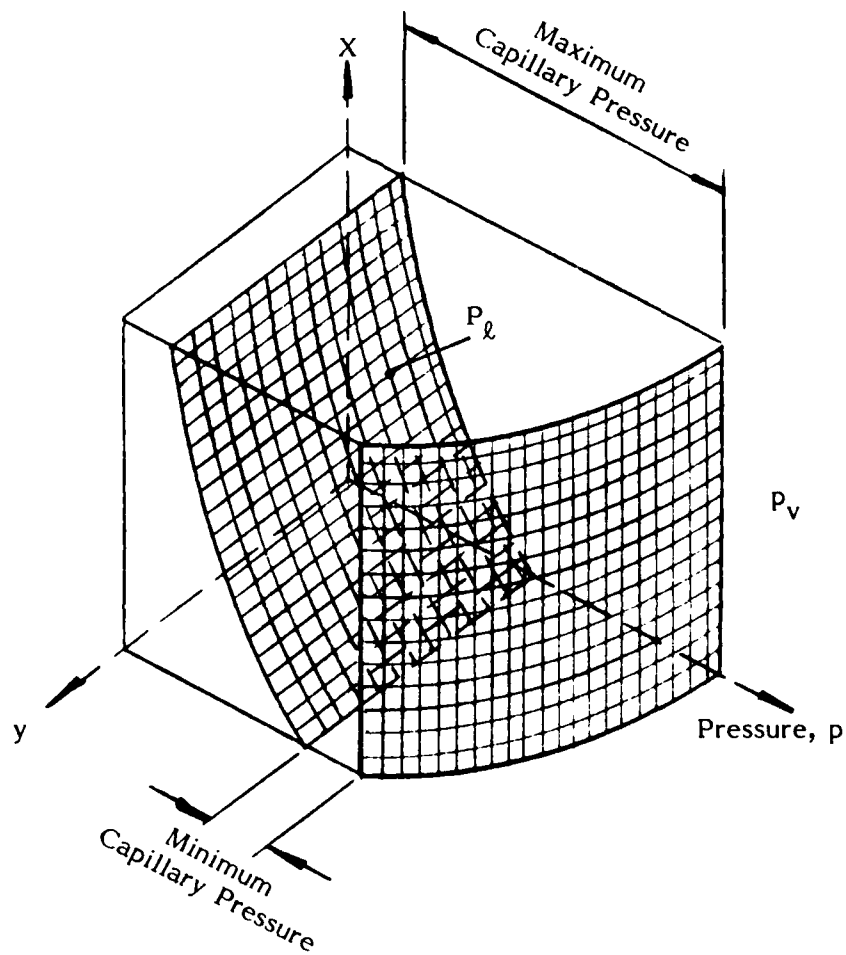


Figure 15

Liquid and Vapor Pressure for a Typical Fin in the STM4-120 EHS Evaporator

satisfied the capillary pumping requirement, however, the chosen configuration was the best compromise among cost, manufacturability and performance. The results of the performance evaluation are summarized in Table 3.

Table 3

Heat Exchanger/Evaporator Construction and Performance Data

Number of fins	= 68
Width/fin	= 2.67 mm
Wall thickness	= 0.2 mm
Wick structure	= 4 layers of 165 mesh, .050 mm (.002") wire diameter
Support structure	= 2 layers of 8 mesh, .48 mm (.017") wire diameter

Operating Data

Heat pipe evaporator temperature	1085°K
Heat input	104 kW
Maximum wick capillary pressure	3200 Pa

Performance

Minimum capillary pressure	650 Pa
Maximum required capillary pressure	2525 Pa
Temperature drop due to:	
Conduction across evaporator wall/wick	1.8 K
Vapor flow restriction in fins	0.4 K
Vapor flow restriction in connecting tubes	2.0 K
Condenser (engine heater)	<u>4.8 K</u>
Total temperature drop	9.0 K
Temperature of inside of wall engine heater tubes	1076°K

SECTION IV

EXTERNAL HEATING SYSTEM CONSTRUCTION

The construction of the EHS was designed to be adaptable to simple folded sheet metal manufacturing techniques. The folded constructions are amenable to robotic welding techniques. In this section, a brief description of the envisioned construction procedure is presented.

1. Construction of the EHS Heat Exchanger/Evaporator

The evaporator construction begins by bonding the layers of wire mesh forming the wick to the sheet that forms the outer wall. The bonded sheet is folded over mandrels of 1.0 mm thickness for the flue gas gap, and 2.0 mm for the sodium vapor gap, resulting in a structure like that shown in Figure 16. The folded sheet is then soaked in solvent to remove the adhesive and any oil or grease.

The folded sheet is then mounted on a special mandrel to perform the squaring operation on the root of the fins as shown in Figure 17. In addition, the edges of the fins are crimped together. This operation permits ready welding of the fin edges without filler rod and simplifies the welding of the roots of the fins to the rest of the enclosure.

The fins are filled with the coarse supporting mesh, then mounted in a welding fixture with heat sinks. At this stage, the fin seams are welded.

Once the fin seams are welded, the assembly is placed in a different welding fixture and the top and bottom covers are welded in place. These covers fit accurately into the squared fin roots, again permitting welding without the use of a filler rod. See Figure 18.

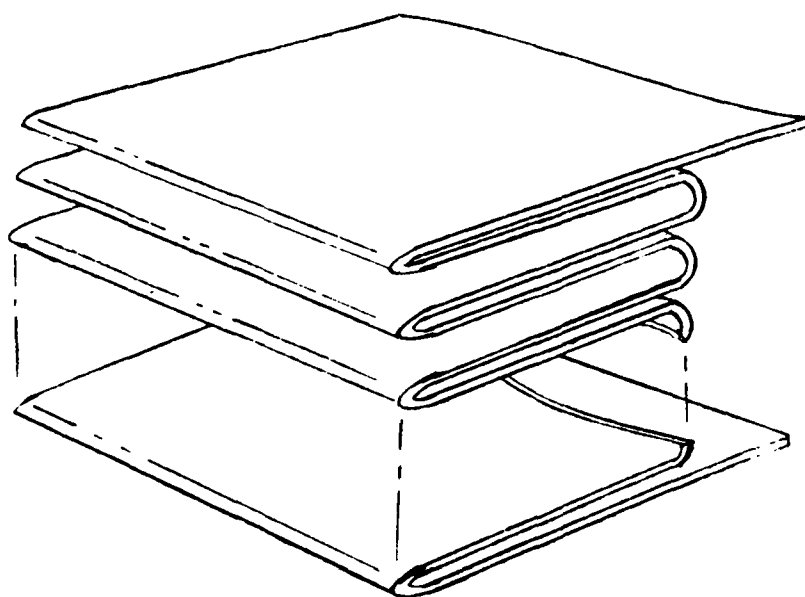


Figure 16
Forming the Evaporator Structure

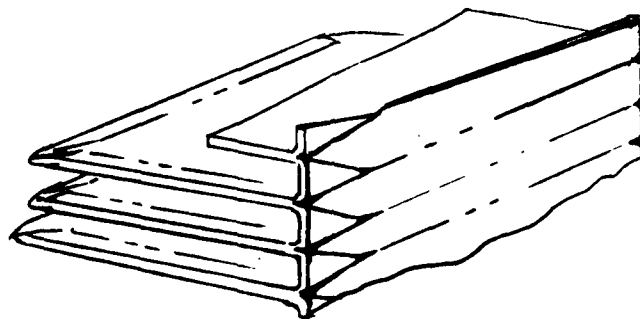


Figure 17
Resulting Fin Shape After Squaring and Crimping

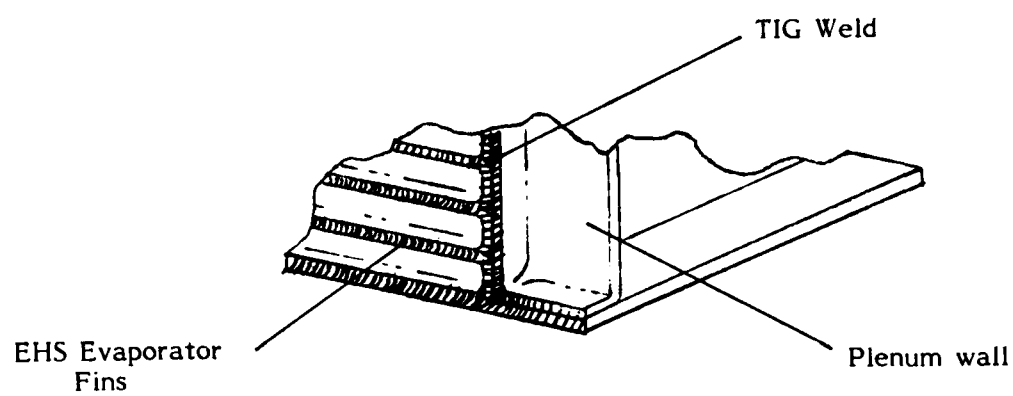


Figure 18

Shape and Fit of Evaporator Plenum Walls to Fin Roots

The final step consists of filling the evaporator plenum, formed by the sides of the outer fins and the top and bottom covers, with coarse supporting mesh, then welding the back plate in place. The pack plate contains the four connecting tubes, with mechanical coupling flanges, that supply the STM4-120 ECU with sodium vapor.

2. Construction of the EHS Recuperator

The techniques used to form the recuperator passages are identical to the initial folding, squaring and seam welding operations used to form the evaporator enclosure.

3. EHS Preliminary Design Drawings

The preliminary design drawings for the complete EHS are included in Appendix E.

4. Heat Exchanger/Evaporator Scale Model Tests

In order to confirm the functionality of the novel evaporator design, scale models were built using the construction techniques outlined above. A photograph of the model is shown in Figure 19.

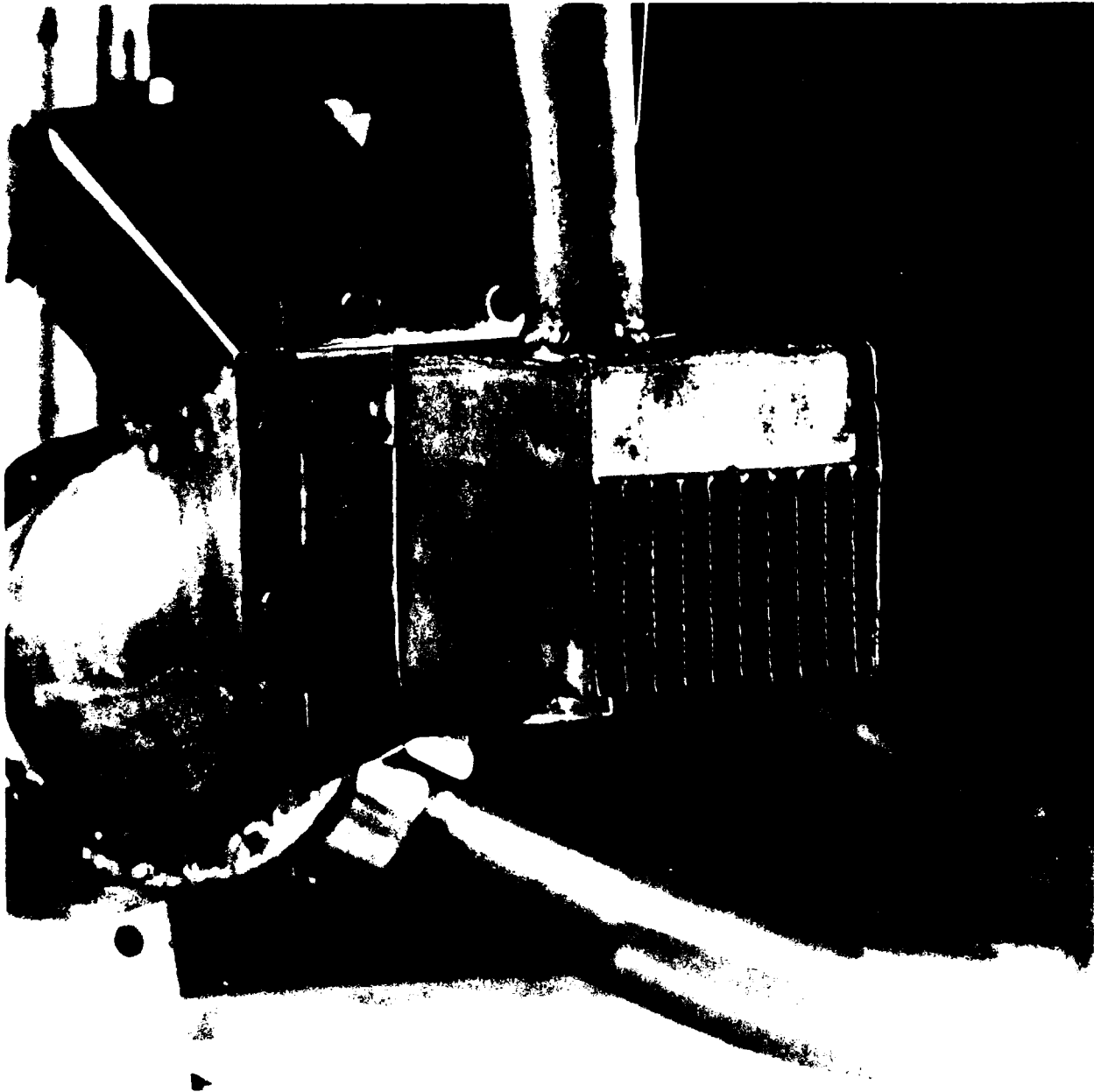


Figure 19

Scale Model of Heat Exchanger/Evaporator

SECTION V

CONCLUSIONS

The conceptual design of the STM4-120 External Heating System appears to be a relatively simple, efficient, and inexpensive system for supplying heat to the Stirling Energy Conversion Unit to provide shaft power for a mobile electric power generator set. In addition, the preliminary design and subsequent scale model testing of the EHS heat exchanger/evaporator substantiate the viability of the conceptual design.

The system optimization resulted in an EHS package size of 330 mm x 250 mm x 70 mm, operating at a full load output of 40 kW with an equivalence ratio of 1.25, 4% atomizing air, fuel consumption rate of 2.67 g/sec, and an EHS exhaust temperature of 225°C.

The analysis of the heat exchanger/evaporator and scale model testing indicate the viability of the evaporator configuration for supplying heat at 800°C to the STM4-120 Stirling engine. The analysis also provides the framework for design algorithms for future designs.

The primary concern of the heat exchanger/evaporator preliminary design was to specify a wick structure capable of providing sufficient liquid distribution within the evaporator fins at an average heat flux of 100 kW/m² and a maximum of 500 kW/m².

Results of the preliminary design yielded an evaporator with 68 fins, each with a wick structure composed of four layers of 165 mesh, .050 mm diameter wire. The fin support structure was composed of two layers of 8 mesh, .43 mm diameter wire. The specified wick, capable of producing 3200 Pa of capillary pressure, was required to produce only 2500 Pa to provide adequate liquid distribution.

While much of the military MEP specifications, MIL-STD-633 and MIL-G-52884 is not applicable to a radically new and different prime mover, such as the STM4-120 Stirling engine, none of the existing design specifications are in conflict with these requirements.

The authors feel that the results of this and related investigations warrant further development of the STM4-120 for Air Force MEP applications. Potential difficulties not accounted for in the preliminary design are problems related to fouling and corrosion.

Counter flow recuperative preheaters have been developed by various manufacturers for gas turbines. These have very similar requirements to those of the EHS recuperator. It is the intention of STM to make use of the know-how of the gas turbine manufacturers, particularly in the areas of fouling and oxidation corrosion of the recuperator and heat exchanger/evaporator, and also in addressing weld or braze joint leakage.

Furthermore, it is possible that proven, available recuperators, metallic or even ceramic, can be directly applicable to the EHS system. This will reduce the technical risk and is thus the preferred approach provided that the system performance does not have to be excessively compromised.

Solutions to these problems require further research and experimental testing and were not within the scope of this effort.

The results of this investigation add further support to the conclusions drawn in the Argonne study, "Base Technology Stirling Engine Military Applications Assessment," listed below:

- Fuel flexibility (similar to that possible with gas turbine sets);

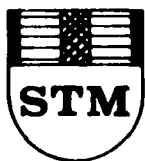
- Low specific weight (comparable with the best achievable with diesel sets);
- Low noise (better than that achievable with silenced diesel sets);
- Low IR - both because the majority of heat is emitted through the radiator at already low temperature and because the engine system is more efficient than current sets and consequently releases less heat; and
- High efficiency (comparable to the best achievable by diesels in this power range).

Stirling Thermal Motors, Inc. is currently engaged in the fabrication of five prototypes of the STM4-120 ECU to establish the predicted performance and reliability of this Stirling engine configuration. This program is expected to continue into 1986, during which prototypes of the EHS design are anticipated to be built and tested.

REFERENCES

1. B. Ziph and T.M. Godett, "Experimental Assessment of Advanced Stirling Component Concepts," Proceedings 22nd. ATD-CCM, October, 1984.
2. R.J. Meijer and B. Ziph, "A New Versatile Stirling Energy Conversion Unit," Paper No. 829299, Proceedings 17th IECEC August, 1982.
3. "Base Technology Stirling Engine Military Applications," Argonne National Laboratories, Report No. AFWAL-TR-84-2016, October, 1983.
4. "Handbook of Heat Transfer," W.M. Rohsenow and J.P. Hartnett, McGraw-Hill, New York, New York, 1973.
5. McAdams, W.H., "Heat Transmission," McGraw-Hill, New York, New York, 1951.
6. Echert, E.G. and Drake, R.M., Jr., "Heat and Mass Transfer," McGraw-Hill, New York, New York, 1959.
7. Hottel, H.C., Williams, G.C. and Satterfield, C.N., "Thermodynamic Charts for Combustion Processes, John Wiley & Sons, New York, New York, 1949.
8. J.E. Kemme, "High Performance Heat Pipes," Thermionic Conversion Specialist Conference--Conference Record, pp. 355-358, Palo Alto, California, 30 Oct. - 1 Nov. 1967.
9. E.K. Levy, "Investigation of Heat Pipe Operating at Low Vapor Pressures," Proceedings of the Annual Aviation and Space Conference, Beverly Hills, California, pp. 671-676, 16 - 19 June 1968.
10. Chi, S.W., "Heat Pipe Theory and Practice," McGraw-Hill, New York, New York, 1976.
11. Dunn, P.D. and Reay, D.A., "Heat Pipes," Pergamon Press, Oxford, United Kingdom, 1978.
12. Marcus, B.D., "Theory and Design of Variable Conductance Heat Pipes," Report No. NASA CR-2018, April, 1972.

APPENDIX A
BREAKTHROUGH IN ENERGY CONVERSION



STIRLING THERMAL MOTORS, INC.

INTRODUCTION

A new concept in Stirling engine technology is embodied in the engine now being developed at Stirling Thermal Motors, Inc. in Ann Arbor, Michigan. This is a versatile engine suitable for many different applications and heat sources.

The engine, rated at 40 kW at 2800 rpm, is a four-cylinder, double-acting variable displacement Stirling engine with pressurized crankcase and rotating shaft seal. It incorporates indirect heating technology with a stacked heat exchanger configuration and a liquid metal heat pipe connected to a distinctly separate combustor or other heat source. It specifically emphasizes high efficiency over a wide range of operating conditions, long life, low manufacturing cost and low material cost.

This article describes the new engine, its design philosophy and approach, its projected performance, and some of its more attractive applications.

BACKGROUND

In 1972, Ford Motor Company obtained a worldwide exclusive license from N.V. Philips of the Netherlands for the Stirling engine, covering virtually all applications, including automotive.

Under this license agreement, the Research Lab at N.V. Philips was to design and build four 175 hp engines, two of which would be

installed in Ford Torino automobiles [1]. See Figures 1 and 2.

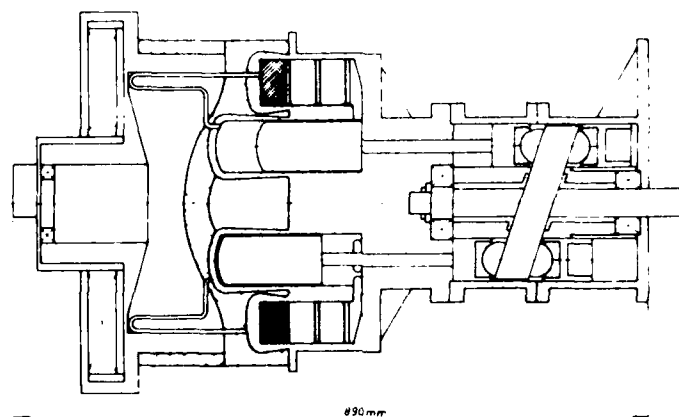


Figure 1

Schematic of the Ford/Philips Torino engine. This is a 4-cylinder double-acting Stirling engine with swashplate drive. Two of the four cylinders and two of the four cooler-regenerator units are shown in cross-section. In these engines the movement of the pistons is transmitted to the main shaft by a swashplate.

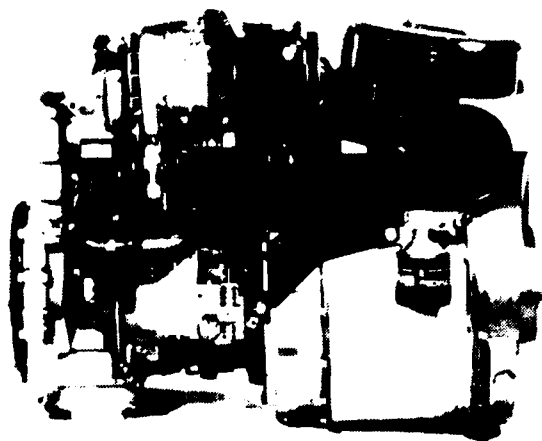


Figure 2

A 175 HP 4-cylinder double-acting type Stirling engine with swashplate drive to be mounted into a Ford Torino automobile (1975).

In 1976 the two Stirling powered Torinos and an older Philips Stirling bus equipped with a 4-cylinder rhombic drive Stirling engine [2] were successfully demonstrated for three days in Dearborn, Michigan.

A few years later, in 1978, Ford terminated its Stirling engine activities to make manpower available for short-term technological problems. A year later, Philips also stopped work on the Stirling engine.

Upon these events, Stirling Thermal Motors, Inc. (STM) was founded in the United States to continue the work done at Philips, so that the results of the years of research and development work done at Philips since its last license agreement in 1968 - which had resulted in a technical breakthrough - would not be lost.

STM's main purpose, from its foundation, was to develop commercial Stirling engines. Philips Laboratories had only made laboratory models for use in research. The only engine made for a special purpose was the one for Ford. When this particular engine was made, Philips was confronted with the practical reality of designing and building a Stirling engine for the most complex application imaginable - an automotive engine. During this time it was discovered that some components of the engine might form obstacles in the way of commercialization because of their complexity and vulnerability.

From 1974 on, real breakthroughs were made in avoiding these complexities. This made a more simple four-cylinder, double-acting Stirling engine possible.

Unfortunately, by this time it was too late to incorporate these improvements into the Ford engine. The intent was to use these new developments in a second-generation Ford engine. This, though, was not

done before Ford dropped its Stirling engine program. The engines being built by earlier Philips licensees were based on designs older than the Ford engine. Their configurations had been frozen for several years. It was therefore impossible to utilize the new improvements.

From the outset STM was convinced that the time was ripe for commercialization of the Stirling engine because all the ingredients for a simple, inexpensive and reliable engine with a long service life were present.

GENERAL APPROACH, BASIC APPLICATIONS

STM's general approach is based on the conclusion that competition with existing internal combustion engines should be avoided, at least in the beginning. Rather, markets should be found where the IC engine cannot be used and where the use of the Stirling engine would be very economical, making use of the unique properties of the Stirling engine. Of the many possible applications, particular attention was given to the following three:

- Prime mover for heat-driven heat pump
- Solar energy conversion
- Engine for generator sets.

If the manufacturing cost of the engine could be sufficiently low, particularly in mass production, the market in these fields alone could be

vast.

TECHNICAL APPROACH

The whole drive of STM is to commercialize the Stirling engine. This means that the engine must be simple, reliable, inexpensive, and that it should have a long service life. None of these requirements should have an adverse effect on the performance of the engine.

More than three years of designing, discussions with suppliers and vendors, component testing and price calculations, led to the new version of the Stirling engine. Studies done for NASA have shown that this engine configuration is suitable for a whole range of power sizes up to 500 hp.

Special emphasis was placed on the flexibility of the engine to adapt readily to a wide range of specific applications, duty cycles and heat sources.

Consequently, indirect heating technology is an integral part of the development effort, making it possible to divide the engine into an energy conversion unit (ECU) and a distinctly separate external heating system (EHS). Different heat sources coupled to the same ECU will adapt the engine to different applications and enhance commercial introduction since most of the development complexity and cost is in the energy conversion unit.

A liquid metal heat pipe [3] is used to transport the heat from the heat source to the expansion heat exchanger of the thermal converter.

So far, most of the development effort has concentrated on the ECU,

which is designated STM4-120 (4 cylinders, 120 cm³ swept volume per piston).
This engine is shown in Figures 3a and 3b.

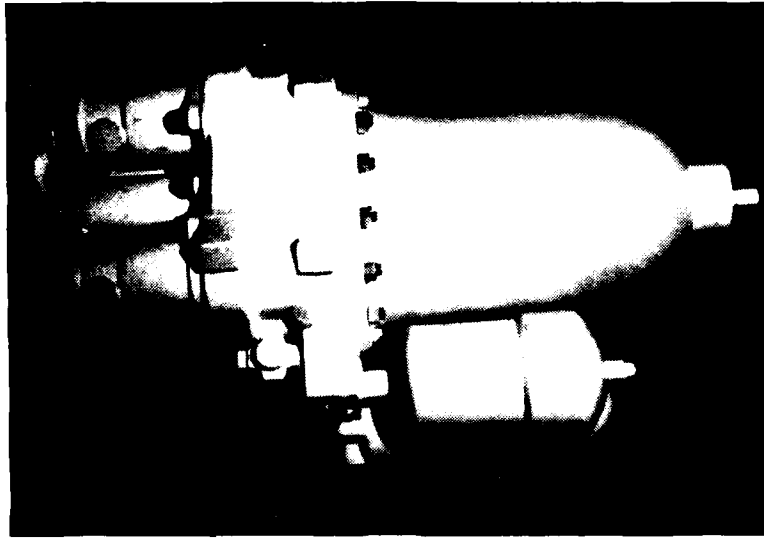


Figure 3a
Full-sized mock-up of the STM4-120

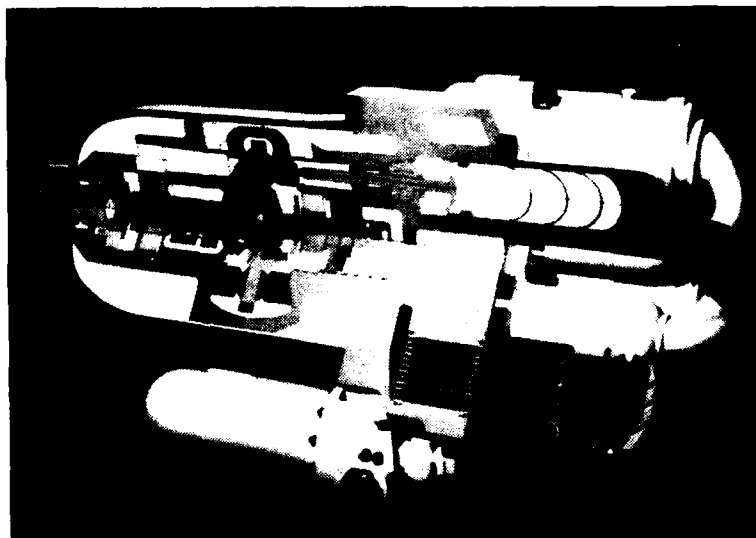


Figure 3b
Cross-section view

ADVANTAGES OF REMOTE HEATING

One of the obstacles in the way of mass production of the Ford/Philips engine was the heater head. This was built as an integrated unit for the four cylinders (Figure 4). The huge mass of heat resistant material was very expensive and made the brazing cycle much too long. The reason for this large amount of material is that the tubular-expansion heat exchanger common to direct flame Stirling engines must accomodate the relatively difficult heat transfer from the flue gas to the walls of the heat exchanger tubes.

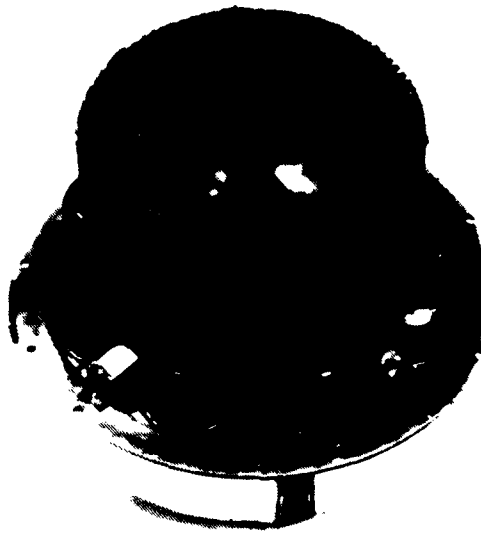


Figure 4

The integrated direct-flame-heated heater head (from the Ford/Philips engine).

It is, therefore, characterized by a complex cage geometry as well as volume and flow-path length which are much larger than those required for the relatively easy heat transfer from the tube walls to the working fluid of the engine.

By contrast, an expansion heat exchanger heated by the condensing metal vapor with a large film coefficient in a heat pipe can be ideally sized to suit the requirements of the working fluid and can be shaped in the most convenient manner for ease of fabrication (Figure 5).

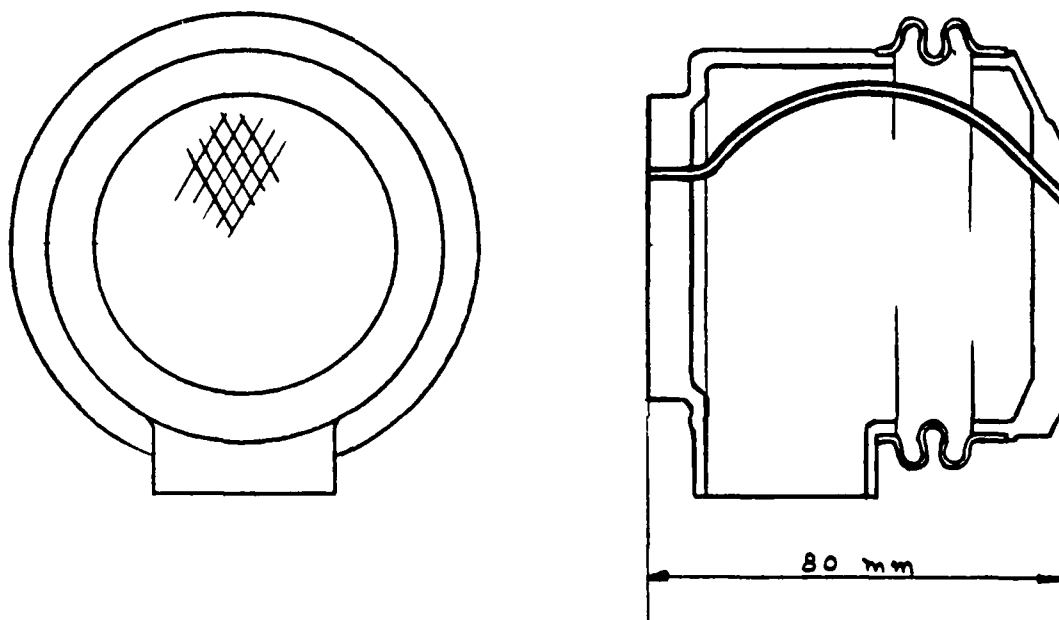


Figure 5

Expansion heat exchangers of the STM4-120. There is one per cylinder. These will later be electron-beam welded in the heat exchanger stack. The tubes are curved, enclosed in a flexible cannister, and brazed to two end plates.

Of course, this itself does not solve the difficult external heat transfer problem, but rather shifts it to the evaporator section of the heat pipe where the size necessary for adequate heat transfer is easily realized since the heat pipe does not have to support the high cycle pressure.

Indirect heating thus offers a number of advantages in addition to

the flexibility with which it endows the engine:

- It brings about major simplifications to the heat-exchanger design. The so-called heat-exchanger-stack configuration, designed to take advantage of the high film coefficient of the condensing metal vapor, is considerably less expensive and more suitable for mass production.
- It brings about considerable improvement of the engine performance by permitting the heater design to be ideally suited to the thermodynamic requirements.
- The uniform temperature throughout the confines of the heat pipe enclosure eliminates hot spots on the heater and thus enhances both the efficiency and the reliability of the engine.

NEW POWER CONTROL SYSTEM

Up to this time, the preferred method for changing power was changing the pressure inside the engine, because the torque of the engine is approximately proportional to the mean pressure of the working gas [4].

The development of this type of power control at Philips was done with a single cylinder displacer engine, where this type of power control was acceptable. However, for a four-cylinder, double-acting engine it became quite cumbersome, particularly when very rapid changes were required, as in automotive applications. This type of system included many check

valves, activator valves, and a storage bottle, along with a high pressure hydrogen compressor.

Figure 6 shows a diagram of the power control system of the Ford/Philips Stirling engine. Power increases when the working gas (in this case hydrogen) is dumped from the high pressure storage bottle into the engine. The reverse takes place when the gas is pumped out of the engine into the storage tank with the high pressure compressor. But because this is a slow process, during this time, a short-circuit power control - which is a loss control - instantaneously cuts the power.

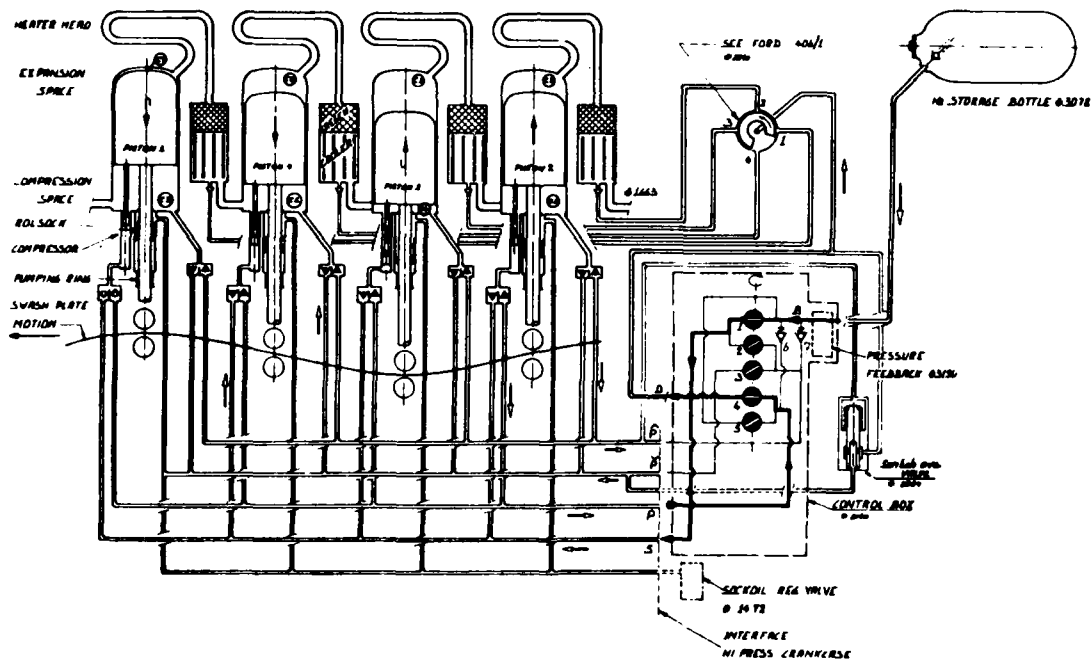


Figure 6

Power control system for the Ford/Philips Stirling engine. the torque of the engine is controlled by the pressure of the working gas. For more power, the working gas from the storage bottle is supplied to the engine. For less power, small hydrogen compressors (connected to the bottoms of the pistons) are pumping the gas out of the engine and back into the storage bottle.

In 1974, during the work on the automotive engine, a relatively simple, heavy duty construction was found to vary the power [5], [6], [7]. In this case the mean pressure of the engine stays the same, but the stroke of the pistons changes. This method of power control has the further advantage of high part load efficiency. Such a construction could be used only with a swashplate drive since the stroke of the pistons is controlled by the angle of the swashplate. It was tested thoroughly in a test rig and applied in the Advenco engine, but the Advenco engine was never adequately tested. Philips eventually sold it to NASA, where further testing was done.

Figure 7 illustrates schematically the variable swashplate mechanism. The swashplate is mounted on a part of the shaft which is tilted an angle α from the main shaft axis. The swashplate is mounted in such fashion that its centerline makes an angle α with the tilted shaft axis and it can be rotated relative to and about the tilted shaft axis in order to change its angle and, with this, the stroke of the pistons.

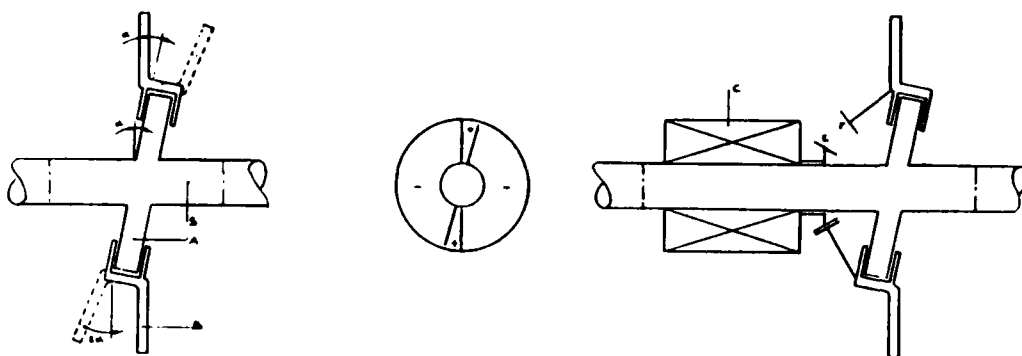


Figure 7 - Schematic of the variable swashplate mechanism, showing the principle of changing the angle of the swashplate, which it makes with the shaft from 0 to 2α . The small plate A is fixed on the shaft S with an angle α . The engine swashplate (drawn here as a solid line) is perpendicular on the shaft S. This situation, $\alpha - \alpha = 0$, means that the strokes of the pistons are zero. When the engine swashplate B is turned 180° relative to the small plate A, the angle then becomes represented by the dotted lines. In this case, the strokes of the pistons are maximal. By turning B relative to A between 0° and 180° any angle of the swashplate between 0 and 2α can be obtained, so the strokes of the pistons can be changed from zero to maximum. C is a hydraulic vane mechanism, the housing of which can turn in one or the other direction depending on which chambers are pressurized and which are not. The oil is fed via two channels in the shaft S. The turning of the housing is transmitted to the engine via bevel gears E and F.

The swashplate angle variation affected by its rotation about and relative to the engine shaft, is accomplished with a rotary actuator. This is a hydraulic vane motor comprising two diametrically opposite vanes attached to the shaft and two attached to the housing as shown in the cross-section of the swashplate-power control of the ECU [8], [9], (Figure 8). Thus, two pairs, A and B, of diametrically opposite chambers are formed. Rotation of the stroke converter housing relative to the shaft is affected by pressurizing one pair and relieving the other. The rotation is transmitted to the swashplate via a bevel gear to which the actuator housing is attached. The supply and return lines to the actuator are concentric tunnels in the shaft connected to a solenoid-actuated proportional valve mounted outside the crankcase. Figure 9 shows a practical model of a variable swashplate in two positions.

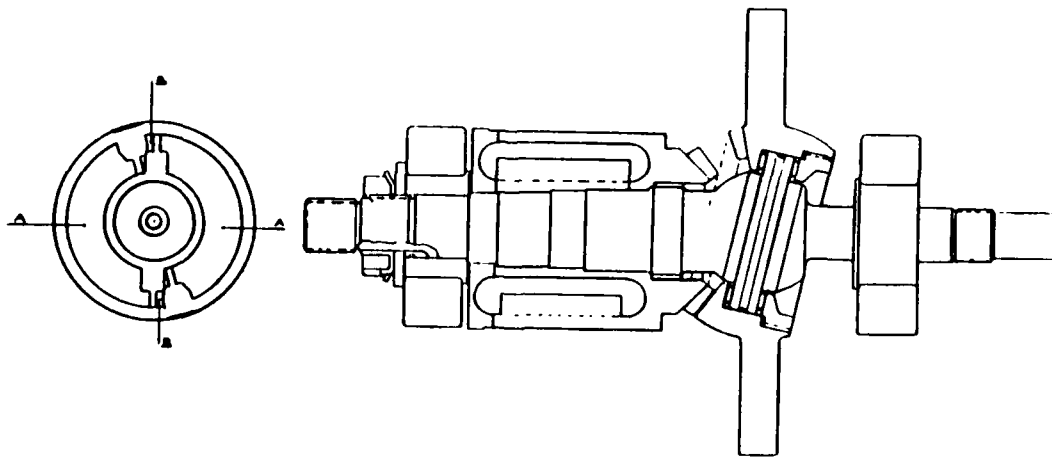


Figure 8

Cross-section of the rotary actuator of the STM-4120. The torque caused by the hydraulic vane motor will turn the swashplate relative to the shaft via pinion and bevel gears.

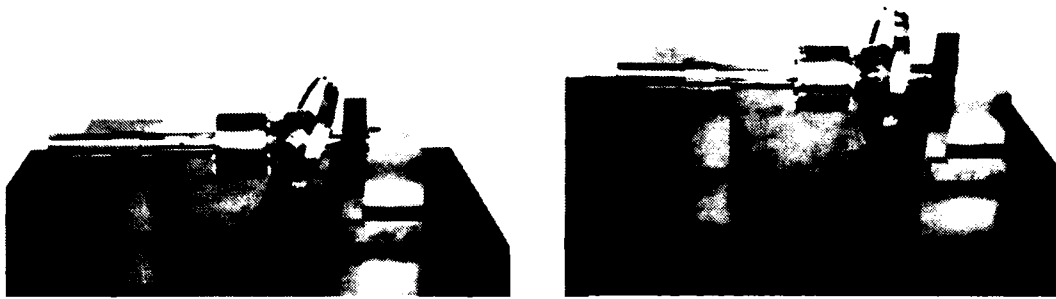


Figure 9

Practical model of a variable swashplate, shown in two positions.

The torque applied by the actuator to the swashplate in order to maintain a certain angular position depends on whether it was rotated to such position in the positive or in the negative direction. Rotation in the negative direction requires less torque since the engine torque itself acts in this case to increase the swashplate angle.

Figure 10 shows the actuator torque as a function of the swashplate angular position relative to the shaft. The curves labeled $M_+(\psi)$ and $M_-(\psi)$ refer to that torque for the positive and negative direction of rotation respectively. The third curve, $\gamma(\psi)$ shows the corresponding swashplate angle. The curve $M_-(\psi)$ reverses its sign within its range of definition. The point of sign reversal is an unstable control point to be avoided by narrowing the range of definition to exclude it. In the

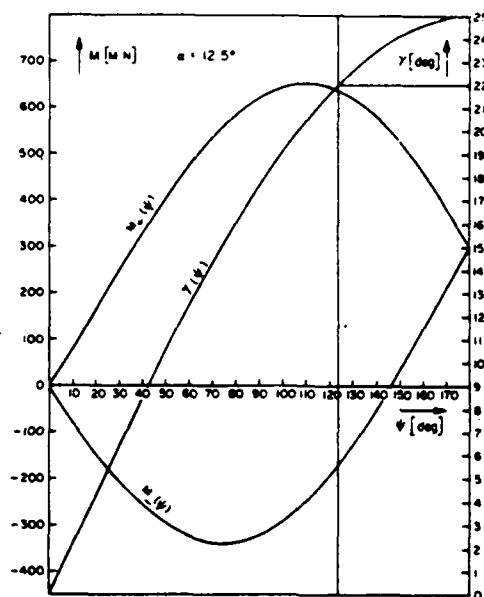


Figure 10

Rotary actuator torque requirements. M_+ means relative rotation for larger stroke in the same direction as the rotation of the engine. M_- means relative rotation for larger stroke in the opposite direction from the rotation of the engine.

Energy Conversion Unit, the angle α is 12.5° , yielding maximum theoretical swashplate angle of $2\alpha = 25^\circ$, corresponding to 180° rotation. The maximum swashplate angle of interest is only 22° , corresponding to a narrower range of definition (124°) in which the torque $M_-(\psi)$ does not change sign.

Loss of hydraulic power will result in the gas forces bringing the swashplate to a position perpendicular to the main shaft axis, reducing the piston stroke to zero - an automatic safety feature.

SEALS

In a four-cylinder, double-acting Stirling engine there are two types of dynamic seals:

- Dynamic seals as piston rings to divide the four cycles from each other, and
- Dynamic reciprocating seals on the piston rods, in order to contain the high pressure working gas in the engine. These seals should also prevent oil penetration into the cylinders from the lubricated drive.

For the dry-running piston rings, a good solution is found in using a reinforced PTFE material.

However, the different types of reciprocating seals for the piston rods are still not reliable. Philips developed the rolling diaphragm seal, but this was shown, in the Ford/Philips engine, to be vulnerable in non-laboratory environments.

STM was able to avoid the gas containment function of these reciprocating seals entirely.

The new power control, with its variable swashplate, made it possible to enclose the relatively small drive with a pressure hull and to use a commercially available rotating shaft seal. Preventing oil penetration into the cylinders is, in this case, much easier and has already been thoroughly tested in other engines.

SPECIAL FEATURES

Amenability to dynamic balancing and the ease of starting the engine are two additional features of the variable swashplate drive and power control elaborated upon in this section.

DYNAMIC BALANCING is achieved by adjusting the swashplate moments of inertia to the reciprocating mass. This is done in a manner enforcing perfect dynamic balance at a certain swashplate angle within its range of variation. At different angles unbalanced moments will appear, but since perfect balance automatically occurs at zero angle, these will be very small.

STARTING of the engine can be accomplished by heating up the expansion heat exchanger and the regenerator and then suddenly using the control pressure to increase the swashplate angle. This will cause the pistons to move in their normal way, causing the engine to immediately develop sufficient power to perpetuate the motion. An accumulator fed by the hydraulic pressure pump will be used for that purpose.

Obviously, such a simple procedure may be used only for such applications as solar conversion since no accessories are required for the combustion. In other cases only a very small starter motor is required to power the accessories needed for combustion, such as the air blower. When the engine has reached its correct temperature the accumulator pressure may be used to quickly increase the angle, having the engine self-start as mentioned above.

DESCRIPTION OF THE ENGINE

A layout drawing of the Energy Conversion Unit is shown in Figure 11.

This unit is distinguished by two major features:

- Variable swashplate drive and power control contained in a pressurized "crankcase" with a commercially available rotating shaft seal containing the working fluid and making it possible to avoid the reciprocating rod sealing problem; and
- Indirect heating, featuring heat-exchanger-stack configuration and liquid metal heat pipe heat transport system.

Following is a brief description of key components.

The rotating shaft seal assembly (1) is bolted to the rear crankcase. The drive shaft (2) is splined to the main shaft to allow for slight deflection or misalignment without affecting the seal performance. The drive shaft is supported radially by one needle and one ball bearing, but since it passes through the pressurized crankcase, it must support the corresponding thrust load. The thrust bearing (3) is a heavy duty tapered roller bearing.

The rotating shaft seal (4) is a commercially available mechanical face seal similar to those found in compressors and gearboxes. The seal is secured in the housing by an interference fit. A rotating mating ring (5) is mounted on the shaft. Both components have an extremely flat, smooth sealing face. When the seal is installed, these faces are pressed together

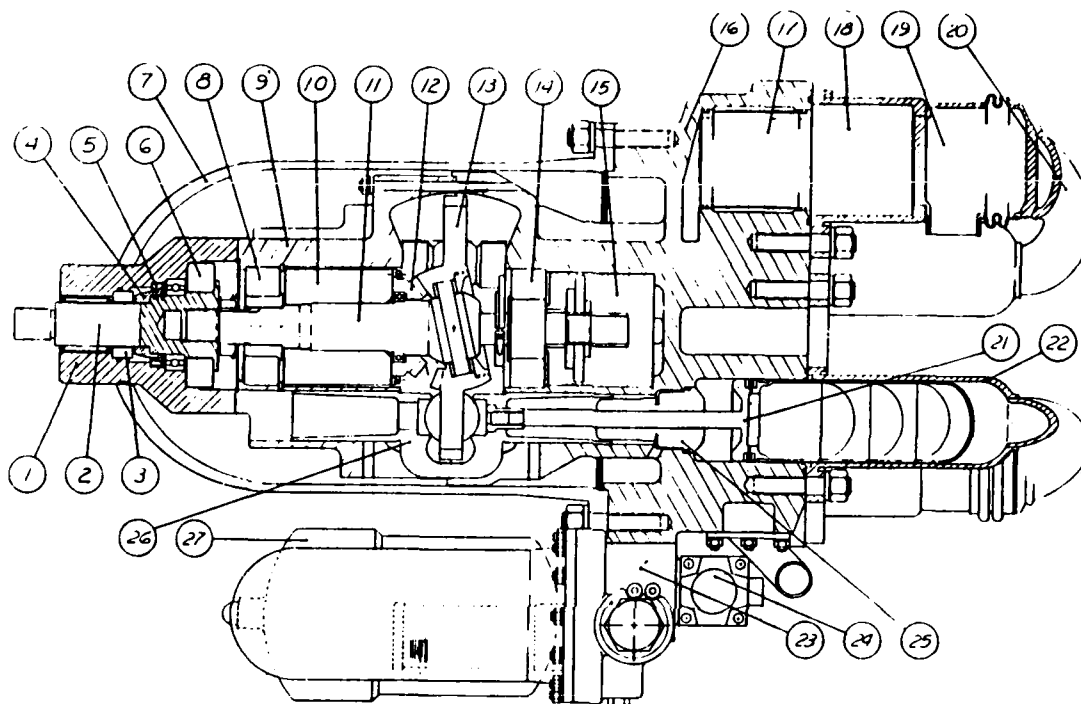


Figure 11

The STM4-120

- | | | |
|---------------------------------|------------------------|-----------------------------------|
| 1) Rotating shaft seal assembly | 10) Rotary actuator | 19) Heater |
| 2) Drive shaft | 11) Main shaft | 20) Hot connecting duct |
| 3) Rotating shaft seal | 12) Bevel gear | 21) Piston assembly |
| 4) Mating ring | 13) Swashplate | 22) Cylinder/regenerator housing |
| 5) Radial lip seal | 14) Front main bearing | 23) Hydraulic service assembly |
| 6) Thrust bearing | 15) Oil pump module | 24) Power control valve |
| 7) Pressure hull | 16) Front crankcase | 25) Oil scraper/cap seal assembly |
| 8) Rear main bearing | 17) Cooler | 26) Crosshead |
| 9) Rear crankcase | 18) Regenerator | 27) Accumulator |

and held in contact by compressed springs in the seal, then surrounded by oil. Because of their closely controlled surface finish, virtually no oil can pass between the sealing faces.

To minimize wear, the seal is hydraulically balanced to reduce contact forces due to crankcase pressure and subjected to a steady flow of oil to maintain cool operation.

The radial lip seal (5) prevents the oil surrounding the rotating shaft seal from draining into the sump.

The pressure hull (7) fits over the rotating shaft seal housing and is bolted to the front of the crankcase, covering the entire drive. The pressure hull serves no structural function other than containing the crankcase pressure.

The front (16) and rear (9) crankcase castings form the major building blocks of the engine, housing the entire drive and power control. In addition, the front crankcase houses the cold thermodynamic system including the coolers, water passages and cold connecting duct. Both are cast from Reynolds 390 Aluminum for reduced weight and suitable running surfaces for the reciprocating components.

The swashplate (13), combined with the main shaft (11) provide the mechanism for converting the reciprocating motion of the pistons into rotary motion. The swashplate is mounted on the shaft in a manner such that relative rotation to the shaft causes the swashplate angle to change.

The front (14) and rear (8) main bearings provide support for the main shaft. The two bearings are spherical roller bearings capable of accomodating the shaft deflection caused by the swashplate loads.

The rotary actuator (10) is a hydraulic vane motor comprising two diametrically opposed vanes attached to the shaft and two attached to the housing, forming two chambers. Rotation of the actuator housing relative to the shaft is accomplished by pressurizing one chamber and relieving the other. The relative rotation between the shaft and actuator housing is transmitted to the swashplate via the bevel gear (12) to change the swashplate angle and therefore the piston stroke.

The oil pump module (15) houses the lubrication and hydraulic pumps which are directly driven by the main shaft. Both pumps are high-efficiency geroters. Internal passages duct the oil to galleries to provide lubrication. High pressure oil is ducted to the externally mounted hydraulic control system and through annular passages in the shaft to the rotary actuator.

The hydraulic service assembly (23) is mounted to the underside of the front crankcase for ready access. It consists of the oil sump, hydraulic accumulator and the power control valve.

The accumulator (27) maintains a large volume of oil at hydraulic system pressure to prevent lags in response to power demands. The accumulator permits use of a smaller pump, thus reducing parasitic losses.

The power control valve (24) is a solenoid activated proportional spool valve that controls the pressure difference across the rotary actuator and in turn, the angle of the swashplate and piston stroke.

The four coolers (17) are conventional tubular heat exchangers mounted in the front crankcase. There is one cooler for each cycle.

The high temperature components consist of identical assemblies for each cycle forming a heat exchanger stack configuration. These components are investment cast from the lower cost iron-based superalloy CRM-6D.

The engine heater (19) is a simple tube bundle heat exchanger consisting of relatively short and small diameter tubes enclosed in a flexible cannister and brazed to end plates. The heater is then electron beam welded to the hot connecting duct (20) and cylinder/regenerator housing (22).

After installation of the regenerator (18), a sintered stack of stainless steel wire mesh, each assembly is mounted on the front crankcase.

The piston (21) is a light weight welded assembly consisting of a base, which houses the dry running piston rings and bearing, welded to the piston rod and dome.

The oil scraper/capseal assembly (25) separates each cycle from the crankcase. The capseal separates the fluctuating cycle pressure from the mean crankcase pressure. The oil scraper is a babbit sleeve radially pressed against the rod. There is no pressure difference across the scraper. Its only function is to prevent oil from penetrating into the cycle. Both the oil scraper and the capseal are mounted in a compliant housing to accomodate the slightly eccentric motion of the piston rod due to the running clearance of the cross head.

The cross heads (26) are made from a high strength aluminum alloy. The extended length reduces side forces and bridge deflection. The running surfaces are treated with a material that is compatible with the Reynolds 390 bore.

The life of the engine is determined by the creep failure life of the hot parts, and is well in excess of 50,000 hours at full load.

Table 1 summarizes some of the important features and parameters of the engine.

Arrangement:	Four double-acting cylinders symmetrically arranged about a common axis. One heat exchanger assembly per cylinder.
Bore:	56 mm
Maximum Stroke:	48 mm
Overall Length:	635 mm
Cross-sectional Dimensions:	Largest cross section is 300 mm in diameter
Total Estimated Weight:	75 kg
Working Fluid:	Helium
Mean Cycle Pressure:	11 MPa
Heater Temperature:	800°C
Power Control:	Piston stroke variation by means of a variable swashplate with a maximum angle of 22°
Heat Transport:	Sodium heat pipe
Gas Containment:	Crankcase pressurized to mean cycle pressure and sealed with a rotating shaft seal
Oil Containment:	Reciprocating rod oil scrapers
Materials:	Iron-base CRM-6D, CG-27 heater tubes

Table 1

Important Features and Parameters of the STM4-120

PERFORMANCE

A set of engine parameters governing the performance of the thermodynamic section was selected for the STM4-120 through an extensive and painstaking effort to tailor the engine performance to the design approach described above.

This approach required a high level of efficiency to prevail over a wide range of operating conditions, making the engine suitable for any duty cycle. Hundreds of different combinations of engine parameters were simulated before the optimal set was selected and established as the design base of the engine.

The result is shown, in Figures 12a and 12b, as two performance maps at mean cycle pressure levels of 11 MPa and 6.3 MPa respectively. Figure 12a shows that between the power levels of 8 kW and 40 kW the shaft efficiency is between 45% and 47% (excluding auxiliaries and collector efficiency). Over a wide power range the efficiency hardly changes with engine speed.

For applications requiring less power, a smaller charge of helium may be used with very little effect on the efficiency. This is shown in Figure 12b for an engine charged to 6.3 MPa to provide power output of no more than 25 kW. This will greatly enhance the life of the engine.

Major contributions to the high efficiency of the engine are derived from the heat-exchanger-stack configuration, the variable stroke power control and the design of the drive mechanism.

The heat-exchanger-stack configuration adds more freedom to the set

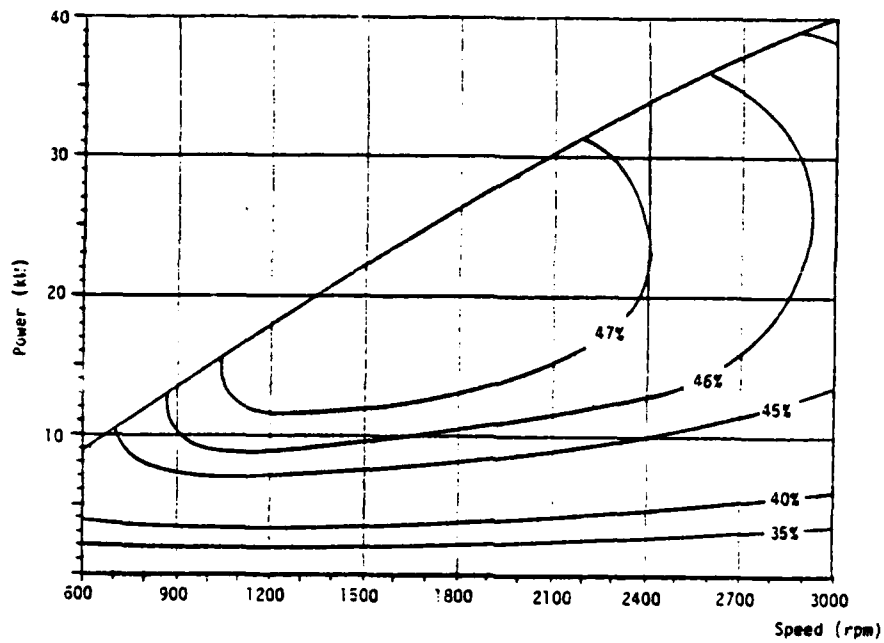


Figure 12a

Performance map of the STM4-120 with mean pressure of 11 MPa showing lines of constant efficiency

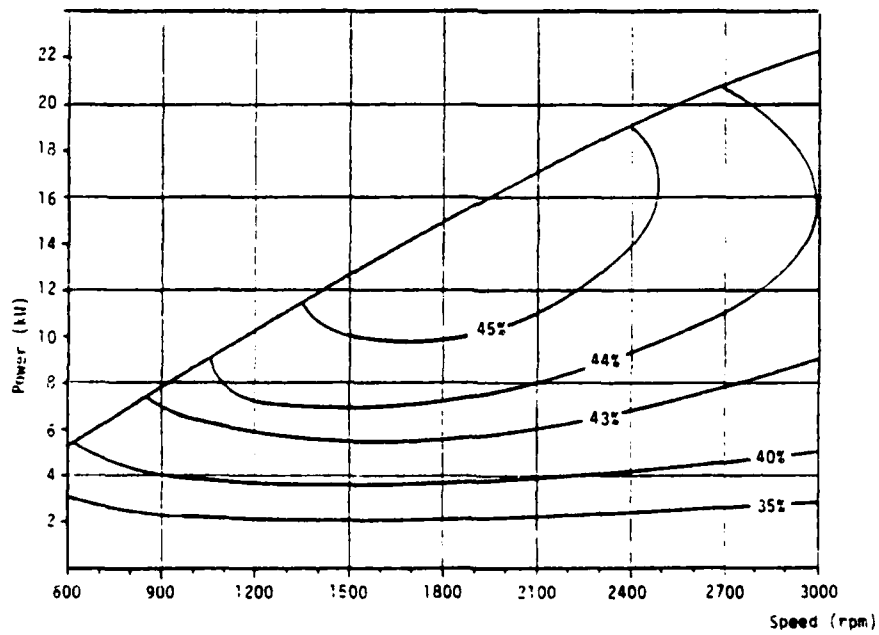


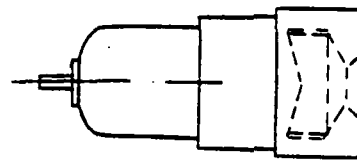
Figure 12b

Performance map of the STM4-120 with reduced mean pressure (6.3 MPa) showing lines of constant efficiency

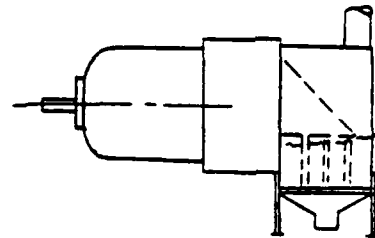
of parameters governing the thermodynamic performance. These can be exploited to facilitate tailoring of the performance characteristics of the engine.

The variable stroke power control inherently inhibits degradation of the efficiency at part load since power reduction is accomplished partly through the addition of void volume or, equivalently, reduction of the pressure wave amplitude, which is beneficial to the indicated efficiency.

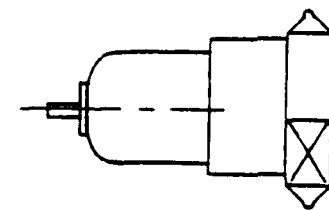
Figure 13 schematically illustrates the ECU with solar receiver, solid fuel combustion, and with a liquid or gaseous fuel combustor.



Solar Receiver



Coal Powder



Liquid and Gaseous Fuels

Figure 13

The STM4-120 with different heat sources

REFERENCES

1. Norman D. Potsma, Ford Motor Company & Rob van Giesel and Frits Reinink, N.V. Philips, Holland, The Stirling Engine for Passenger Car Application, Paper 730648, SAE, Chicago, Illinois, June 1973.
2. R.J. Meijer and C.L. Spigt, Philips Research Labs, Eindhoven, The Potential of the Philips Stirling Engine for Pollution Reduction and Energy Conservation. Paper presented at the Second Symposium on Low Pollution Power Systems Development, organized by the Committee on the Challenge of Modern Society of the North Atlantic Treaty Organization in Dusseldorf, Germany, November, 1974.
3. G.A.A. Asselman and D.B. Green, Heatpipes I & II, Philips Technical Rev.33, 104-113, Nov. 1973 No. 4 and 138-148, 1973, No. 5.
4. R.J. Meijer, The Philips Hot Gas Engine with Rhombic Drive Mechanism, Philips Techn. Rev. 20, 245-262, 1958/9, No.9.
5. R.J. Meijer and A.P.J. Michels, Conceptual Design of a Variable Displacement Stirling Engine for Automotive Propulsion, Paper 789351, Proceedings, 13th IECEC, October 1978.
6. J. Vos, Design Characteristics of an Advanced Stirling Engine Concept, Paper 799257, Proceedings 14th IECEC, Boston, August 1979.
7. R.J. Meijer and B. Ziph, A Variable Angle Wobble Plate Drive for a Stroke Controlled Stirling Engine, Paper 799258, Proceedings, 14th IECEC, Boston, August 1979.
8. R.J. Meijer and B. Ziph, Variable Displacement Automotive Power Train, Proceedings, 5th International Automotive Propulsion Systems Symposium, Dearborn, MI, April 1980.
9. B. Ziph and R.J. Meijer, Variable Stroke Power Control for Stirling Engines, Paper 810088, SAE, Detroit, Michigan, February 1981.
10. Roelf J. Meijer and Benjamin Ziph, A New, Versatile Stirling Energy Conversion Unit, Paper 829299, Proceedings, 17th IECEC, Los Angeles, California, August 1982.

APPENDIX B
PREHEATER AND EVAPORATOR HEAT TRANSFER ANALYSIS

List of Symbols

A	Heat transfer area [m^2] (for gap: $dA = 2w dx$)
g	Gap width [m]
h	Heat transfer coefficient [$\frac{\text{W}}{\text{m}^2 \text{ } ^\circ\text{C}}$]
k	Thermal conductivity [$\frac{\text{W}}{\text{m } ^\circ\text{C}}$]
\dot{m}	Mass flow [kg/sec] per gap
Nu	Nusselt number (for gap: $Nu = hg/k$)
\dot{Q}	Heat flow (Watts)
T	Temperature ($^\circ\text{C}$)
t_w	Preheater plate wall thickness (m)
w	Depth of heat exchanger (or preheater) gap (m)
x	Coordinate in the flue gas flow direction (m)
φ	Specific enthalpy (J/kg)

Subscripts

f	denotes properties of the flue gas
a	denotes properties of the incoming air
w	denotes properties of the heat exchanger wall material

Governing Equations for Preheater Heat Transfer Analysis

The analysis is performed on a counterflow, flat plate recuperator with multiple parallel gaps of width (g), depth (w) and length (ℓ).

Laminar flow is assumed throughout the gaps and hence the Nusselt number (based on the gap width) is constant:

$$Nu = \frac{h}{k} g = 3.8 \quad (1)$$

The analysis, performed on a single gap, takes into account the variation of fluid properties with temperature, but not with pressure.

The functional relationship of the thermal conductivity (k) and the enthalpy (φ) to the temperature T for both flue gas and incoming air is known for the particular fuel used and the equivalence ratio. The latter relation takes into account molecular dissociation.

The energy balance for the flue gas requires that heat loss from the flue gas by convection and conduction to the incoming air stream be equal to the reduction in enthalpy of the flue gas stream:

$$\dot{Q}_f = \frac{-(T_f - T_a) dA}{\frac{1}{h_f} + \frac{tw}{k_w} + \frac{1}{h_a}} = m_f d\phi_f (T_f) \quad (2)$$

Observing that $dA = 2wdx$, substituting (1) in (2) and rearranging, we

have:

$$\dot{m}_f \left\{ \frac{g}{Nu} \left[\frac{1}{k_f(T_f)} + \frac{1}{k_a(T_a)} \right] + \frac{t_w}{k_w} \right\} \frac{d\varphi_f(T_f)}{dx} + 2w(T_f - T_a) = 0 \quad (3)$$

Similarly, energy balance for the air stream requires that:

$$d\dot{Q}_a = \dot{m}_a d\varphi_a(T_a) \quad (4)$$

$$\text{but} \quad d\dot{Q}_a = -dQ_f = \dot{m}_f d\varphi_f(T_f) \quad (5)$$

hence:

$$\dot{m}_a \frac{d\varphi_a(T_a)}{dx} = -\dot{m}_f \frac{d\varphi_f(T_f)}{dx} \quad (6)$$

Equations (3) and (6) form a set of two coupled, first order, non-linear ODE's for the two unknown functions $T_f(x)$ and $T_a(x)$. The boundary conditions are the known inlet temperatures $T_f(0)$ and $T_a(l)$ of the flue gas and air streams respectively.

Governing Equations for the Heat Exchanger/Evaporator Analysis

The analysis is performed on a heat exchanger with flat parallel gaps (of width g , depth w , and length l) through which flue gas flows laminarly at a constant Nusselt number $Nu = 3.8$. The gas yields its heat to the gap walls which are at constant and uniform temperature t_w .

AD-A173 813

STIRLING ENGINE EXTERNAL HEAT SYSTEM DESIGN WITH HEAT
PIPE HEATER(U) STIRLING THERMAL MOTORS INC ANN ARBOR MI
T M GODETT ET AL. JUL 86 AFMAL-TR-86-2018

2/2

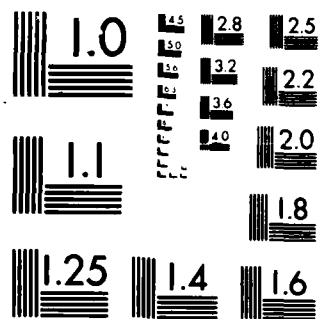
UNCLASSIFIED

MIPR-FY-1455-84-N0618

F/G 21/7

NL





MICROCOPY RESOLUTION TEST CHART
NATIONAL BUREAU OF STANDARDS 1963-A

As before, energy balance on the flue gas requires:

$$d\dot{Q}_f = -h_f(T_f - T_w) dA = \dot{m}_f d\phi_f(T_f) \quad (7)$$

Substitution of

$$Nu = \frac{h_f g}{k_f}$$

and of

$$dA = 2w dx$$

in (7) yields:

$$\dot{m}_f \frac{d\phi_f(T_f)}{dx} + 2w Nu \frac{k_f(T_c)}{g} (T_f - T_w) = 0 \quad (8)$$

This first order, non-linear ODE in the unknown function $T_f(x)$ forms the mathematical model of the evaporator/heat exchanger. The boundary condition is the known inlet temperature $T_f(o)$ which is the flame temperature.

APPENDIX C
EHS ANALYSIS CODE SAMPLE RUN

EHS Analysis Code Listing

Fuel Data

HTCR atomic ratio of hydrogen to carbon in fuel
SLHV specific lower heat value of fuel, cal./gr.

Operating Data

ER equivalence ratio
AAR atomizing air to intake air ratio
TPA initial guess for preheated air temperature, °K
MFUEL fuel consumption rate, gr./sec.
TWEX outside wall temperature of evaporator °K
TAIN air intake temperature °K

Geometric Data; Heat Exchanger (see figure)

EXL length, m
WEX width, m
NGEX number of flue gas passages ("gaps")
GEX gap width, m
NUEX Nussel number
THM wall thickness, m
CM thermal conductivity of the metal, w/m °K

Geometric Data; Preheater (see figure)

PL length, m
WP width, m
NGP number of flow passages for each stream
GPA gap width, air side, m
GPF gap width, flue side, m
NUP Nusselt number

Cold Start Data

ROM density of the metal, gr/cm³
CAPM specific heat of the metal, cal./gr. °K
ETHG effective gauze thickness: the thickness of a solid sheet
 of metal of the same weight per unit area as the gauze
 stack, m

Numerical Data

NEX	number of discrete steps in heat exchanger calculation
NPA	number of discrete steps in preheater calculation
EPSP	maximum convergence error in preheater iterative procedure, relative
EPS	maximum convergence error in EHS iterative procedure relative

SAMPLE RUNS - AUGUST 8, 1985

Run #1 (gauge not taken into account in CSP calculations)

```

1.8040      10179.
1.2500      .40000E-01 949.90      2.0000      1075.0      301.00
.12000      .60000E-01 61 .13000E-02 3.8000      .30000E-03 21.600
.18000      .60000E-01 78 .13000E-02 .13000E-02 3.8000
8.0000      .12000      .00000
100 100 .20000E-02 .20000E-02
PREHEATED AIR TEMP.      949.9 K
FLAME TEMPERATURE      2374.9 K
HEAT EXCHANGER OUTPUT TEMP.      1096.3 K
HEAT OUTPUT      74.661 kw
EXHAUST OUTLET TEMP.      569.9 K
E.H.S. EFFICIENCY      87.675 %
COLD START PENALTY      45.389 gr
PRESSURE DROP      2.193 KPa
FLOW FRICTION POWER      296.791 w
623.38      841.16      1388.4

```

B>A:PRINT EHS.FOR

Not ready error reading drive A
 Abort, Retry, Ignore? R

B:EHS .FOR is currently being printed

B>

```

3: 0.12,0.06, 61 1.3E-3,3.8,0.3E-3,21.6,
4: 0.18,0.06, 78 1.3e-3,1.3e-3,3.8,
5:* 8.0,0.12,0.537E-3,
6: 100 100 0.002,0.002

```

*E

Run #2 (gauge taken into account)

```

B>EHS
1.8040      10179.
1.2500      .40000E-01 949.90      2.0000      1075.0      301.00
.12000      .60000E-01 61 .13000E-02 3.8000      .30000E-03 21.600
.18000      .60000E-01 78 .13000E-02 .13000E-02 3.8000
8.0000      .12000      .53700E-03
100 100 .20000E-02 .20000E-02
PREHEATED AIR TEMP.      949.9 K
FLAME TEMPERATURE      2374.9 K
HEAT EXCHANGER OUTPUT TEMP.      1096.3 K
HEAT OUTPUT      74.661 kw
EXHAUST OUTLET TEMP.      569.9 K
E.H.S. EFFICIENCY      87.675 %
COLD START PENALTY      87.361 gr
PRESSURE DROP      2.193 KPa
FLOW FRICTION POWER      296.791 w
623.38      841.16      1388.4

```

B>

End of input file

*6

6:* 100 100 0.002,0.002
6:* 200 200 0.002,0.002

*E

B>EHS

Run #3 step size decreased

1.8040	10179.				
1.2500	.40000E-01	949.90	2.0000	1075.0	301.00
.12000	.60000E-01	61	.13000E-02	3.8000	.30000E-03 21.600
.18000	.60000E-01	78	.13000E-02	.13000E-02	3.8000
8.0000	.12000	.53700E-03			
200	200	.20000E-02	.20000E-02		
PREHEATED AIR TEMP.			950.5 K		
FLAME TEMPERATURE			2374.9 K		
HEAT EXCHANGER OUTPUT TEMP.			1097.2 K		
HEAT OUTPUT			74.613 kw		
EXHAUST OUTLET TEMP.			570.4 K		
E.H.S. EFFICIENCY			87.618 %		
COLD START PENALTY			87.187 gr		
PRESSURE DROP			2.179 KPa		
FLOW FRICTION POWER			293.849 w		
624.00	837.51	1383.4			

B>

3:* 0.12,0.06, 61 1.E-3,3.8,0.3E-3,21.6,

*

4:* 0.18,0.06, 78 1.3e-3,1.3e-3,3.8,
4:* 0.18,0.06, 78 1.e-3,1.e-3,3.8,

*E

B>EHS

Run #4 gap decreased

1.8040	10179.				
1.2500	.40000E-01	949.90	2.0000	1075.0	301.00
.12000	.60000E-01	61	<u>.10000E-02</u>	3.8000	.30000E-03 21.600
.18000	.60000E-01	78	<u>.10000E-02</u>	<u>.10000E-02</u>	3.8000
8.0000	.12000	.53700E-03			
200	200	.20000E-02	.20000E-02		
PREHEATED AIR TEMP.			976.9 K		
FLAME TEMPERATURE			2382.0 K		
HEAT EXCHANGER OUTPUT TEMP.			1082.8 K		
HEAT OUTPUT			76.464 kw		
EXHAUST OUTLET TEMP.			532.0 K		
E.H.S. EFFICIENCY			89.792 %		
COLD START PENALTY			85.233 gr		
PRESSURE DROP			4.493 KPa		
FLOW FRICTION POWER			578.828 w		
645.59	818.03	1319.2			

APPENDIX D
DEVELOPMENT OF EHS EVAPORATOR PRESSURE DROP EQUATIONS

List of Symbols and Abbreviations

m	Mass flow rate
b	Width
l	Length
Q	Heat flow
A	Area
v	Velocity
ρ	Density
λ	Heat of vaporization
P	Pressure
g	Acceleration of gravity
τ	Shear stress
r	Radius
Re	Reynolds number
f	Drag coefficient
θ	Angle of liquid flow to horizontal
ϵ	Porosity
K	Permeability
F	Friction coefficient
D	Dynamic drag coefficient
x,y	Position
β	Profile coefficient for momentum flow

Subscripts

l	Liquid
v	Vapor
w	Wick
h	Hydraulic

The analysis is performed on a finned heat pipe evaporator with N_f fins, length ℓ , width b , and thickness t , as shown in Figure C-1.

From conservation of mass:

$$\frac{d\dot{m}_\ell}{dx} + \frac{d\dot{m}_v}{dx} = 0 \quad (1)$$

From conservation of energy:

$$\left. \frac{d\dot{m}_v}{dx} \right|_y = \left(\frac{y}{b} \right) \left(\frac{1}{\ell} \right) \frac{\dot{Q}}{\lambda} \quad (2)$$

Combining Equations 1 and 2 and integrating yields:

$$\dot{m}_\ell = \left(1 - \frac{x}{\ell} \right) \frac{\dot{Q}}{\lambda} \quad (3)$$

From conservation of mass:

$$\dot{m} = \rho A_v \quad (4)$$

Combining Equations 2 and 4 yields an expression for vapor velocity:

$$v_v = \frac{y/b \cdot \dot{Q}}{\rho_v A_v \lambda} \quad (5)$$

Combining Equations 3 and 4 yields an expression for liquid velocity:

$$v_\ell = \frac{\left(1 - \frac{x}{\ell} \right) \dot{Q}}{\rho_\ell A_\ell \lambda} \quad (6)$$

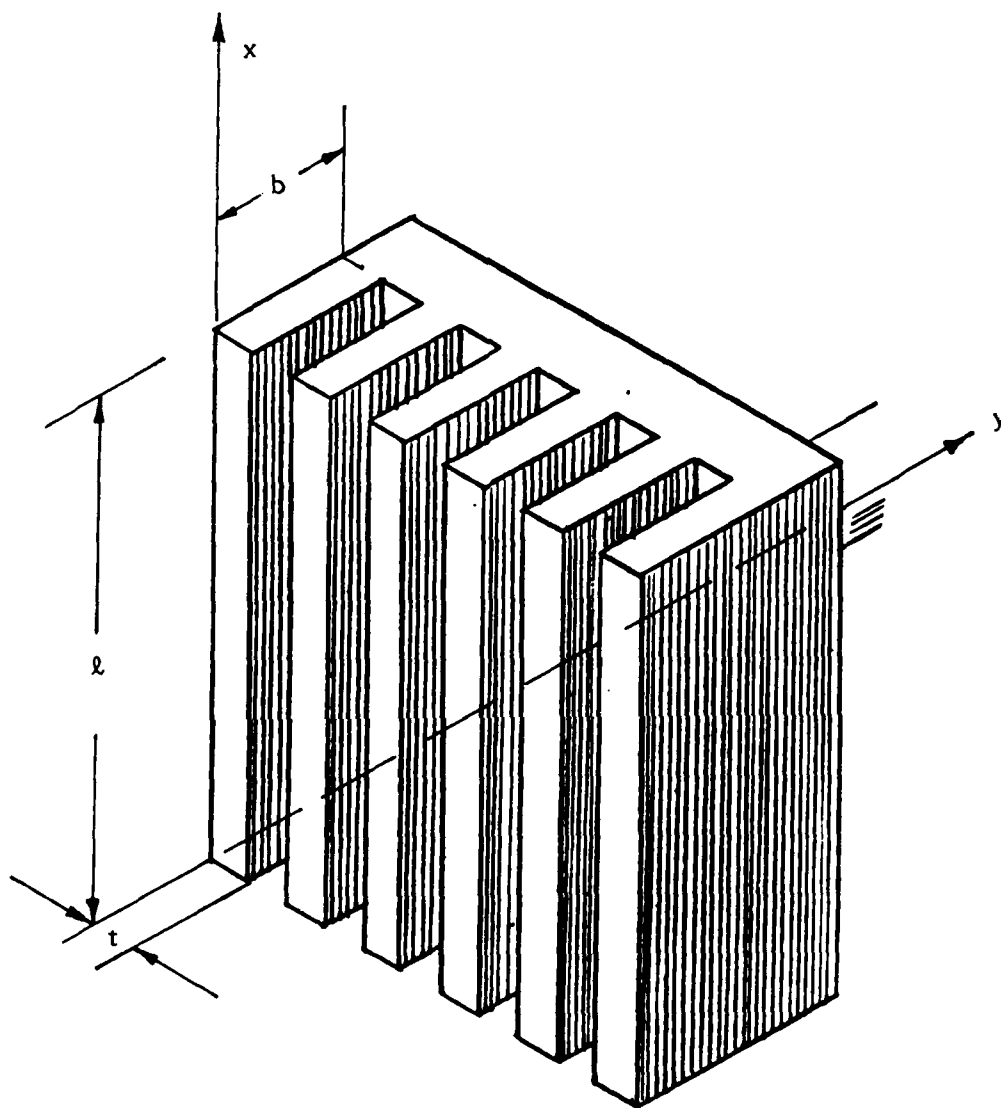


Figure D-1

EHS Heat Exchanger/Evaporator Geometry

From conservation of momentum, the steady state liquid pressure gradient in the evaporator wick in the direction of liquid flow is:

$$\frac{dP_l}{dx} = - \frac{2 \tau_l}{r_{h,l}} \pm \rho_l g \sin \theta \quad (7)$$

where the first term is due to flow resistance and the second term is due to gravity.

Introducing Reynolds number and drag coefficient;

$$Re_l = \frac{2r_{h,l} \rho_l v_l}{\mu_l} \quad (8)$$

$$f_l = \frac{2 \tau_l}{\rho_l v_l^2} \quad (9)$$

Combining Equations 7, 8, and 9 yields:

$$\frac{dP_l}{dx} = - (f_l Re_l) \frac{\mu_l v_l}{2r_{h,l}} \pm \rho_l g \sin \theta \quad (10)$$

Introduce wick porosity, ϵ and wick area, A_w ;

$$A_l = A_w \epsilon \quad (11)$$

Define wick permeability, K ;

$$K \equiv \frac{2 \epsilon r_{h,l}^2}{(f_l Re_l)} \quad (12)$$

Combining Equations 6, 10, and 12 yields:

$$\frac{dP_l}{dx} = \frac{-\mu_l}{K A_w \lambda \rho_l} \left(1 - \frac{x}{l} \right) \dot{Q} \pm \rho_l g \sin \theta \quad (13)$$

Define friction coefficient, F_ℓ ; and substituting into Equation 13;

$$F_\ell \equiv \frac{\mu_\ell}{KA_w \lambda \rho_\ell} \quad (14)$$

$$\frac{dP_\ell}{dx} = -F_\ell \dot{Q} \left(1 - \frac{x}{\ell} \right) - \rho_\ell g \sin \theta \quad (15)$$

Integrating Equation 15 yields an expression for the liquid pressure drop (including the hydrostatic term) as required for evaluating the capillary pressure in Equation 18 in the text.

From conservation of momentum, the vapor pressure drop can be expressed as follows:

$$\frac{dP_v}{dy} = \frac{-(f_v Re_v) \mu_v \dot{m}_v}{2A_v r_v^2 \rho_v} - \beta \frac{2\dot{m}_v}{A_v^2 \rho_v} \frac{d\dot{m}_v}{dy} \quad (16)$$

The construction of the fin is such that the vapor path is packed with a porous screen structure to provide structural support to the fin walls. This support structure is analagous to the screen wick used for the liquid flow, with regard to the flow resistance since it can be shown that the vapor flow is laminar and incompressible (see Appendix D). Therefore, by introducing the vapor screen permeability, K_v , and vapor screen porosity ϵ_v , Equation 16 becomes;

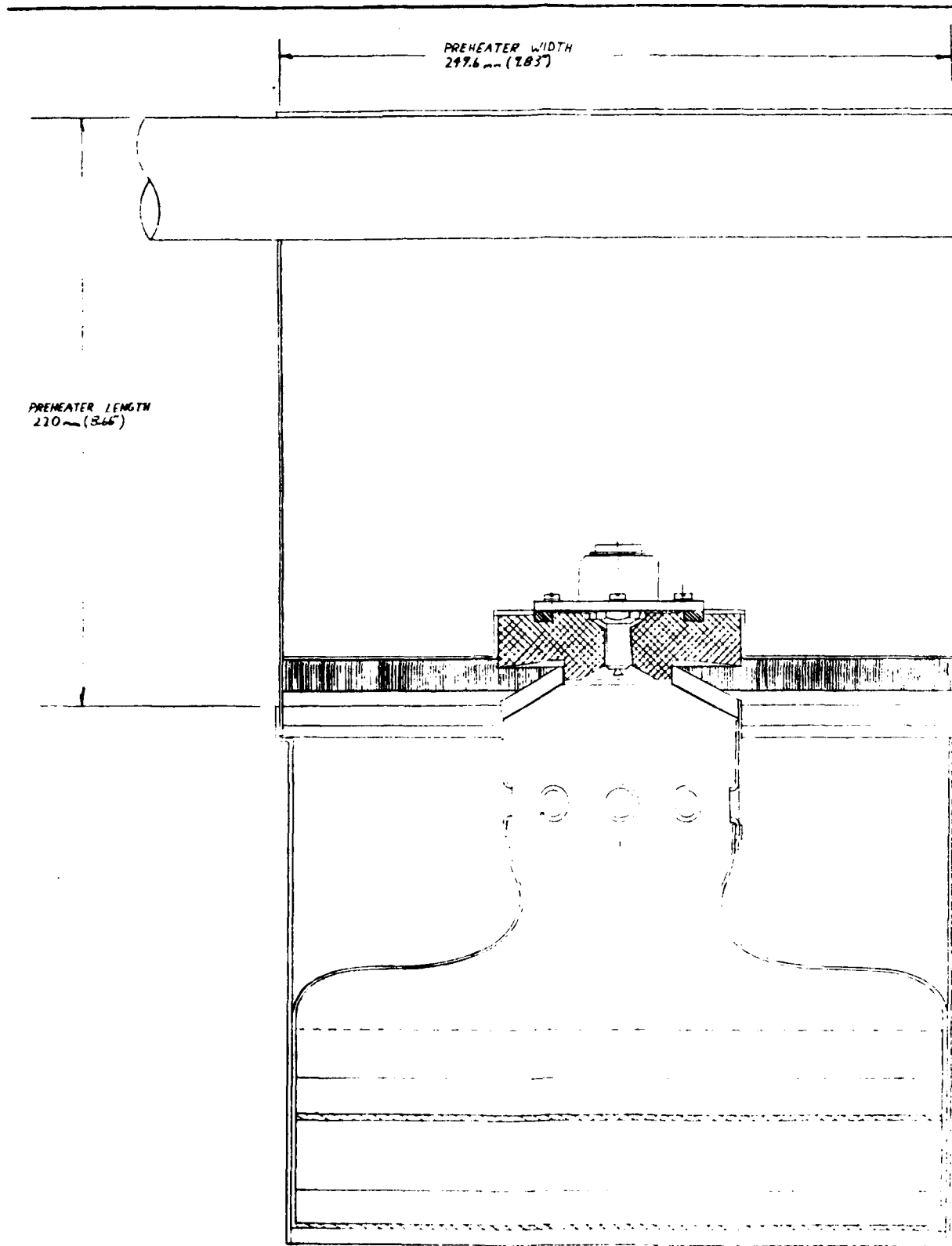
$$\frac{dP_v}{dy} = - \left[\frac{\mu_v}{KA_v \lambda \rho_v} \right] \frac{y}{b} \dot{Q} - \left[\frac{\beta}{A_v^2 \rho_v \lambda^2} \right] 2 \left(\frac{y}{b} \right) \dot{Q} \quad (17)$$

Introducing the vapor friction coefficient, F_v and the vapor drag coefficient, D_v yields

$$\frac{dP_v}{dy} = -F_v \dot{Q} \left(\frac{y}{b} \right) - 2D_v \frac{\dot{Q}^2}{b} \left(\frac{y}{b} \right) \quad (18)$$

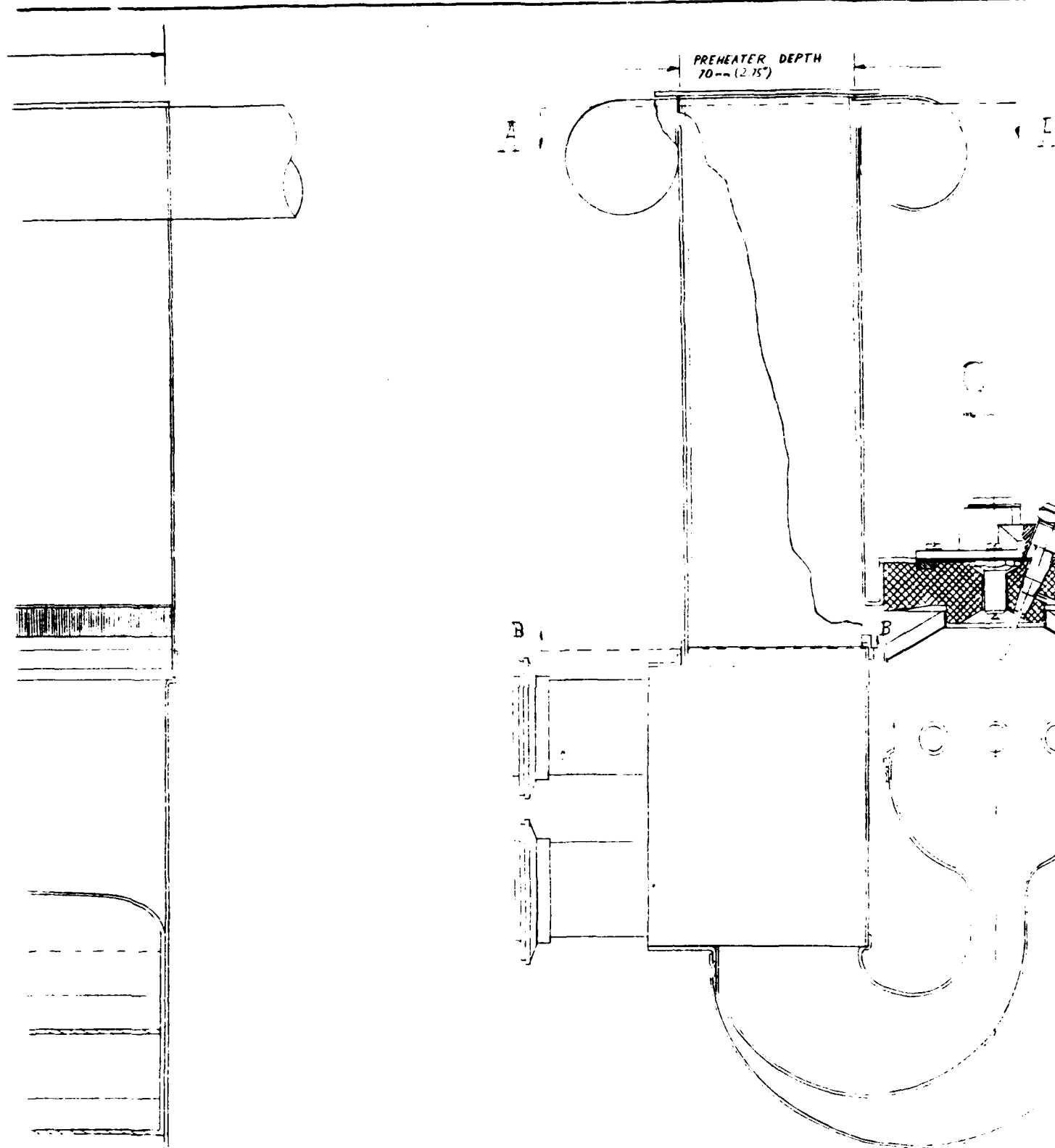
Integrating Equation 18 yields an expression for the vapor pressure drop as required for evaluating the capillary pressure in Equation 18 in the text.

APPENDIX E
PRELIMINARY DESIGN DRAWINGS



Reproduced from
best available copy.

1.3

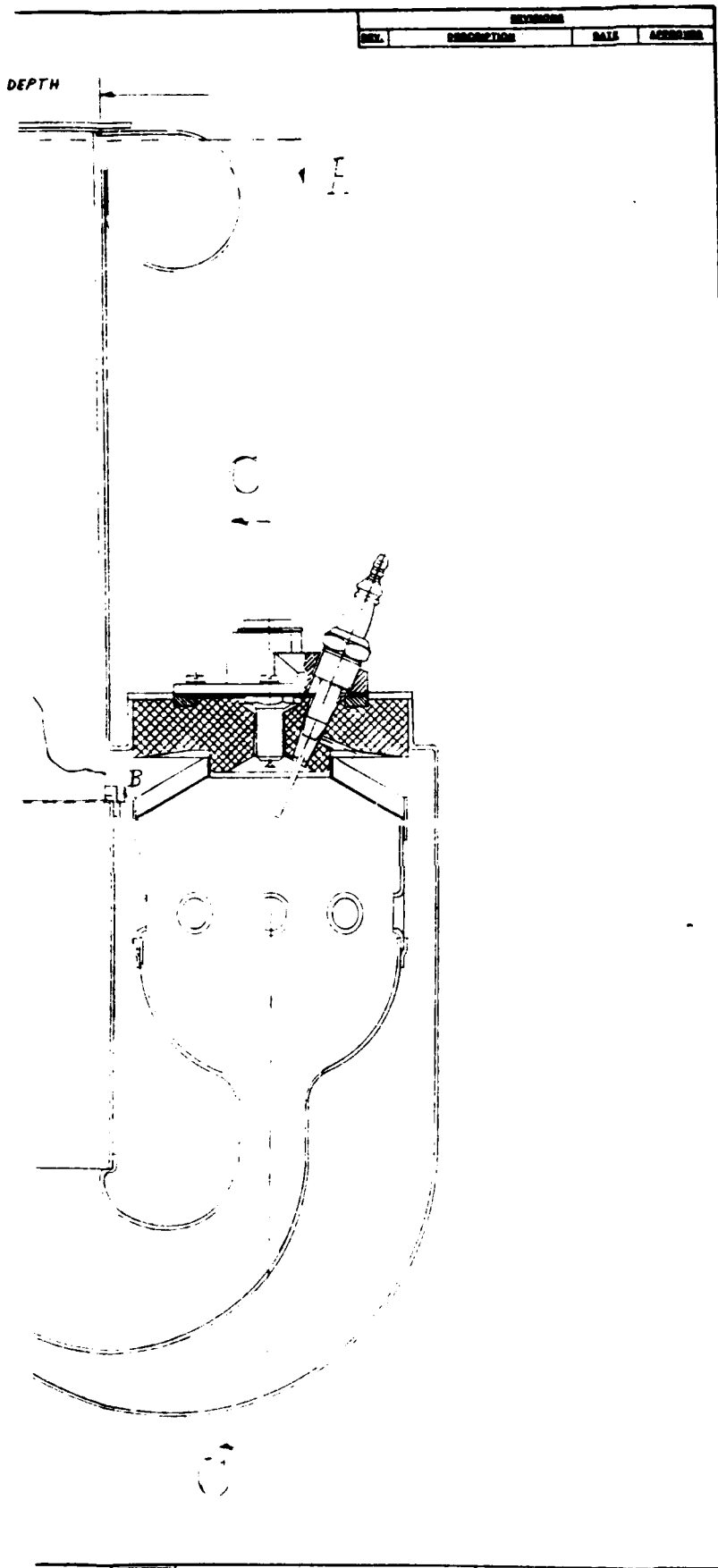



NOTES: 1. CR. 1111-15

Property of Stirling Thermal Motors, Inc.



PART NAME
STM 4120 E
STIRLING THERMAL



	PART NAME	PART NO.	Sheet No.	FORM
	STM 4-120 EHS	70108	1 of 3	D
STIRLING THERMAL MOTORS, INC. <small>1841 Dearborn St. Chicago 48, Ill. U.S.A. Tel. 312 999-1700</small>				

303

Reproduced from
best available copy.

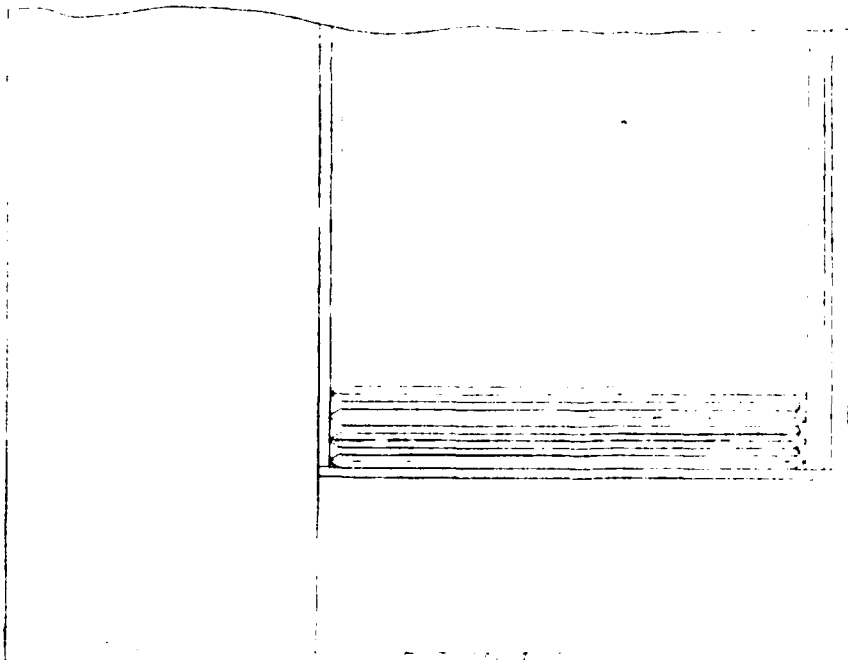
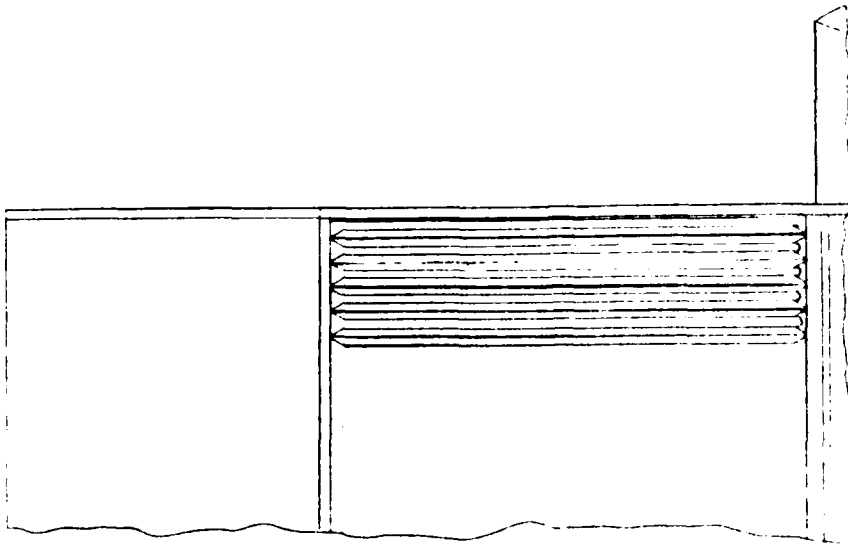
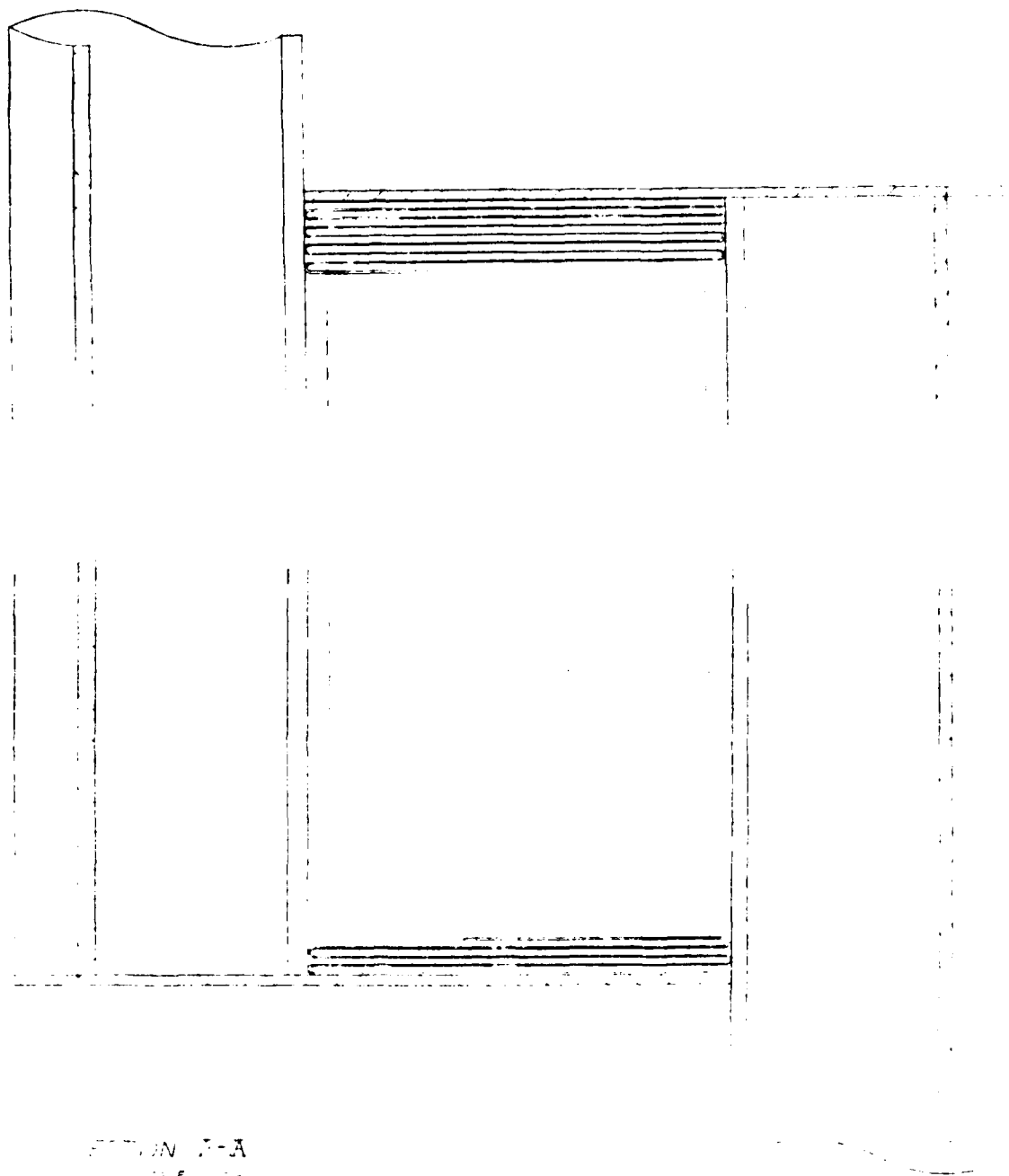


FIGURE 1

REVISION			
REV.	DESCRIPTION	DATE	APPROVED



SECTION 7-A
PRE-HEATER

NOTES: 1. 11-85



PART NAME
STM 4-120 LHS PRE-HEATER

PART NO
70108

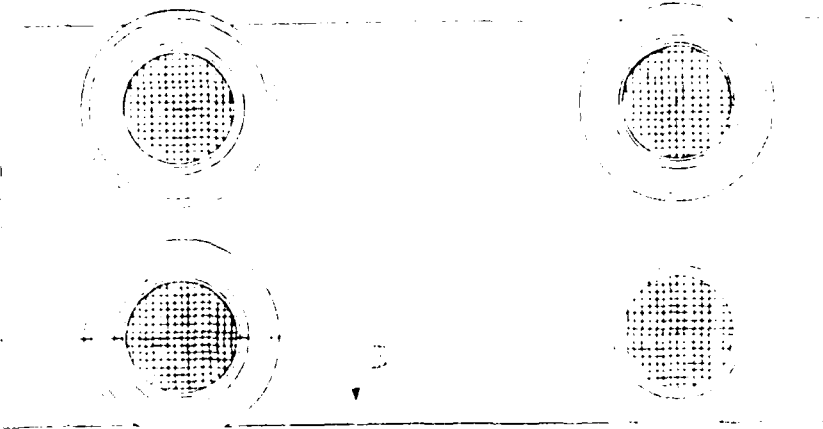
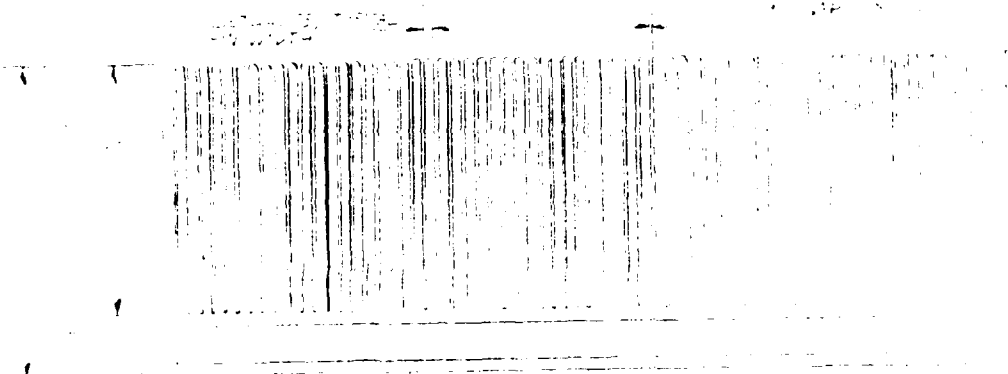
Rev: 1.0
2.0, 3.0

Property of Stirling Thermal Motors, Inc.

STIRLING THERMAL MOTORS, INC.

1001 Oak Street
Ann Arbor, Michigan 48106-1500
Tel: 313-960-1100

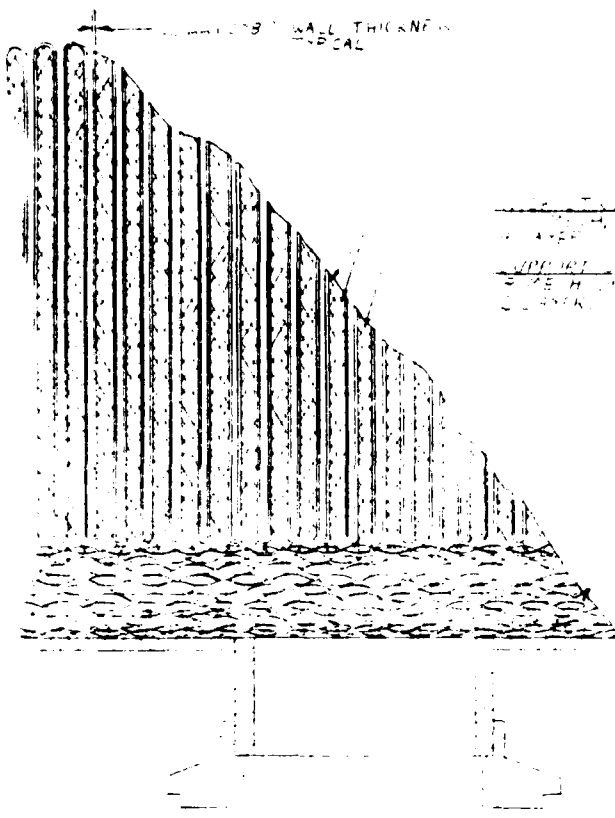
232



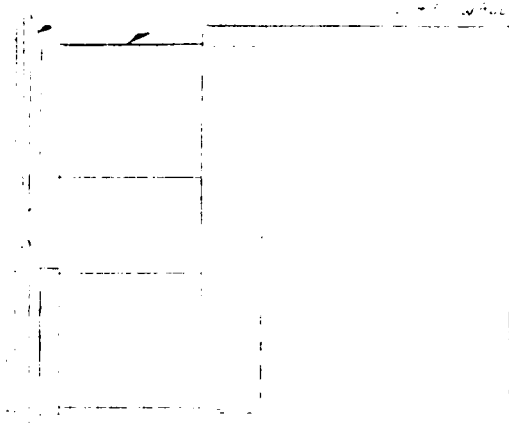
Reproduced from
best available copy.

1082

REVISIONS			
REV.	DESCRIPTION	DATE	APPROVED



STIRLING THERMAL MOTORS, INC.
P.O. BOX 1000
ALBUQUERQUE, N.M. 87106
TELEPHONE (505) 261-1000
FAX (505) 261-1001



NOTES	PART NAME	PART NO.	SHOP NO.
	STIRLING THERMAL MOTORS, INC.	10100	



STIRLING THERMAL MOTORS, INC.

2082

END

12-86

DTIC